

# Cosmic Reionisation by Stellar Sources: Population II Stars

Aaron Sokasian<sup>1</sup>, Tom Abel<sup>2</sup>, Lars Hernquist<sup>1</sup>, and Volker Springel<sup>3</sup>

## ABSTRACT

We study the reionisation of the Universe by stellar sources using a numerical approach that combines fast 3D radiative transfer calculations with high resolution hydrodynamical simulations. By supplementing a *one-step* radiative transfer code specifically designed for following ionisation processes with an adaptive ray-tracing algorithm, we are able to significantly speed up the calculations to the point where handling a vast number of sources becomes technically feasible. This allows us to study how dim low-mass sources, excluded in previous investigations owing to computational limitations, affect the morphological evolution of the reionisation process.

Ionising fluxes for the sources are derived from intrinsic star formation rates computed in the underlying hydrodynamical simulations. Analysis of numerically converged results for star formation rates and halo mass functions allows us to assess the consequences of not including low-mass objects and enables us to correct for resolution effects. With these corrections, we are able to reduce the effective mass resolution limit for sources to  $M \sim 4.0 \times 10^7 h^{-1} M_{\odot}$ , which is roughly an order of magnitude smaller than in previous studies of this kind. Our calculations reveal that the process by which ionised regions in the IGM percolate is complex and is especially sensitive to the inclusion of dim sources. Moreover, we find that given the same level of cosmic star formation, the number of ionising photons required to reionise the Universe is significantly overestimated if sources with masses below  $\sim 10^9 h^{-1} M_{\odot}$  are excluded. This result stems from the fact that low-mass sources preferentially reside in less clumpy environments than their massive counterparts. Consequently, their exclusion has the net effect of concentrating more of the cosmic ionising radiation in regions which have higher recombination rates.

---

<sup>1</sup>Harvard-Smithsonian Center for Astrophysics, 60 Garden Street, Cambridge, MA 02138, USA

<sup>2</sup>Department of Astronomy and Astrophysics Penn State University, 525 Davey Lab, University Park, PA 16802, USA

<sup>3</sup>Max-Planck-Institut für Astrophysik, Karl-Schwarzschild-Straße, 1, 85740 Garching bei München, Germany

We present the results of our reionisation simulation assuming a range of escape fractions for ionising photons and make statistical comparisons with observational constraints on the neutral fraction of hydrogen at  $z \sim 6$  derived from the  $z = 6.28$  SDSS quasar of Becker and coworkers. We find that given the amplitude and form of the underlying star formation predictions, an escape fraction near  $f_{esc} = 0.10 - 0.20$  is most consistent with the observational results. In these models, reionisation is expected to have occurred between  $z \sim 7 - 8$ , although the IGM remains fairly opaque until  $z \simeq 6$ .

Our method is also capable of handling the simultaneous reionisation of the helium component in the IGM, allowing us to explore the plausibility of the scenario where sources with harder spectra are primarily responsible for reionisation. In this case we find that if the sources responsible for reionising hydrogen by  $z \sim 8$  had spectra similar to AGNs, then the helium component of the IGM should have been reionised by  $z \sim 6$ . We find that such an early reionisation epoch for helium does not necessarily conflict with observational constraints obtained at  $z \simeq 3$ , but may be challenged by future observations at higher redshifts.

The recent WMAP measurements of the electron scattering optical depth ( $\tau_e = 0.17 \pm 0.04$  according to the “model independent” analysis of Kogut et al.) appear to be inconsistent with the relatively late onset of reionisation by the normal population II type stars that we consider. In order to simultaneously match the observations from the  $z = 6.28$  SDSS quasar and the optical depth measurement from WMAP with the sources modeled here, we require an evolving escape fraction that rises from  $f_{esc} = 0.20$  near  $z \simeq 6$  to  $f_{esc} \gtrsim 10$  at  $z \sim 18$ . Such a steep enhancement in the stellar production rate of ionising photons would be consistent with an IMF that becomes more and more top heavy with increasing redshift.

*Subject headings:* radiative transfer – diffuse radiation – intergalactic medium – galaxies: quasars

## 1. INTRODUCTION

The nature of the sources responsible for ionising the neutral hydrogen in the intergalactic medium (IGM) has been the subject of a long-standing debate. There are both observational and theoretical indications that some or perhaps all of this ionising

background comes from stars and not hard sources, such as quasars. While it seems clear that quasars provide a significant contribution to the ionising background at low redshifts,  $z \sim 3$ , the steep drop in the abundance of bright quasars at earlier times brings into question whether they are capable of maintaining the ionised state of the IGM at  $z \gtrsim 4 - 5$ . In an earlier paper (Sokasian et al. 2003), we showed that the observed opacities in both H I and He II indicate that quasars alone cannot produce the required emissivity to match observations at  $z \simeq 4$ . The situation is exacerbated at higher redshifts where observations by Fan et al. (2000), Becker et al. (2001), and Djorgovski et al. (2001) imply that the IGM was highly ionised at  $z \simeq 6$  even though the emissivity from bright quasars was likely unimportant. Given this discrepancy, it appears that a substantial portion of the ultraviolet photons at  $z > 4$  were produced by an additional class of sources.

It has been argued that star forming galaxies may yield the required ionising emissivities (e.g. Haehnelt et al. 2001, Bianchi et al. 2001, Steidel et al. 2001), although it is possible that harder low-luminosity active galactic nuclei (AGN) may also make up the difference (Haiman & Loeb 1998). Early star formation also provides a possible explanation for the widespread abundance of metals in the IGM (Cowie et al. 1995) while reionisation by faint AGNs may provide a more plausible solution if the escape fraction for stellar radiation from galaxies is restrictively small (Schirber & Bullock 2002, Wood & Loeb 2000).

There have been numerous studies of cosmological reionisation using semi-analytical methods (e.g. Haardt & Madau 1996, Madau et al. 1999, Chiu & Ostriker 2000, Valageas & Silk 1999). In these models, the impact of the UV background is treated using a spatially and directionally averaged radiative transfer equation which incorporates the mean luminosity function per unit volume for the source term and the statistical properties of absorbing clouds for the recombination term. Inevitably though, to accurately address questions related to the time-dependent propagation of radiation fronts, especially during the early stages of the reionisation process where the radiation field is highly inhomogeneous, a detailed radiative transfer approach is required. This has proved to be an extremely challenging endeavour owing to the high dimensionality of the problem. A brief review of the problem and the various techniques which have been employed in recent years is presented in Razoumov et al. (2002).

One of the major challenges involved with such exercises is determining how to efficiently process the large number of sources that may be responsible for reionisation. In the case of bright quasars, the associated number density is small enough that straightforward approaches can be employed (e.g. Sokasian et al. 2001, 2002). The situation becomes much more difficult when galaxies are the primary sources. For typical cosmologies, a  $10^3 \text{ Mpc}^3$  comoving volume can easily harbour  $> 10^4$  star forming galaxies

by  $z = 6$ .

Tracking the ionising flux from such a large pool of sources over many time steps inevitably requires the implementation of sophisticated algorithms designed to efficiently process the cumulative effects from each source. By combining a photon conserving algorithm with two independent hierarchies of trees, one for rays (Abel & Wandelt 2002) and one for the sources themselves, Razoumov et al. (2002) were able to improve the efficiency of the calculations to study the inhomogeneous process of reionisation from star forming sources down to a redshift of  $z = 4$ . In particular, they were able to carefully follow time-dependent radiative transfer calculations on a uniform  $128^3$  Cartesian grid representing a volume with a comoving length of  $L \sim 7h^{-1}$  Mpc on each side which stored the results of pre-computed hydrodynamical simulations of galaxy formation. As a result of their calculations, the authors were able to address a number of questions related to the morphological evolution of the reionisation process. In particular, they showed a picture of stellar reionisation in which photons initially do not travel far from ionising sources, in contrast to images from simulations by Gnedin (2000).

More recently, Ciardi et al. (2003b) combined high-resolution N-body simulations and a semi-analytic model of galaxy formation with a Monte Carlo radiative transfer code to study reionisation in a volume with a comoving length of  $20h^{-1}$  Mpc. In their analysis they assessed the effect of the environment by performing a subsequent simulation on a smaller  $10h^{-1}$  Mpc comoving box centered on a cluster. They found that the environment where the radiation is produced modifies reionisation through the influence of the density dependence of the recombination rates. This conclusion raises the question of whether the exclusion of the copious number of dim low-mass sources which fall below the resolution limit of these simulations may play a more important role in determining the morphological evolution of the reionisation process. The fact that most models of galaxy formation predict that the bulk of the resultant ionising radiation is produced in relatively massive systems has provided some motivation for ignoring the low-mass sources altogether, especially in lieu of the high computational cost of radiative transfer calculations. However, since dim low-mass sources reside in relatively less clumpy environments compared to their brighter counterparts, their overall contribution to the ionising emissivity in the IGM may be significant in spite of their intrinsic faintness.

We examine the impact of low-mass sources by conducting very fast radiative transfer calculations capable of processing a large number of sources from high resolution hydrodynamic simulations. In particular, by supplementing our previous *one-step* radiative transfer code (see Sokasian et al. 2001) with an adaptive ray tracing algorithm we are able to significantly speed up the calculations to the point where handling more than  $10^5$

sources becomes technically feasible. Our cosmological simulation is taken from a high resolution run in a series of calculations performed by Springel & Hernquist (2003a), and utilises  $2 \times 324^3$  particles in a box of comoving length  $L \sim 10h^{-1}$  Mpc. Radiative transfer calculations are then performed on a  $200^3$  grid where we store the corresponding density fields at each redshift. This allows us to simulate reionisation with a source mass resolution that is about an order of magnitude below the limit of the Ciardi et al. (2003b) simulations. Furthermore, the use of a  $200^3$  grid offers a factor of  $\sim 4$  improvement in spatial resolution for the same box length. It is also important to point out that by using hydrodynamics to describe the gas physics, rather than an N-body simulation, we are able to estimate the clumping on unresolved scales in our grid by computing the spatial distribution of particles within a given cell (see Sokasian et al. 2001). This represents an important advantage over the density interpolation schemes associated with N-body codes which smooth out density variations on sub-grid scales. As a result we expect to more properly account for the recombination rates in high density regions where clumping is important.

In the present paper, which is part of a series examining reionisation, we focus on the redshift interval  $z \simeq 20$  to  $z \simeq 6$  with specific interest in how the level of cosmic star formation predicted in the comprehensive set of hydrodynamic simulations conducted by Springel & Hernquist (2003a) performs in the context of observational constraints on the opacity of the IGM at  $z \simeq 6$ . Our method also treats the simultaneous reionisation of helium in the IGM, allowing us to explore the plausibility of the scenario where AGNs are primarily responsible for reionisation.

Here, we restrict our attention to sources of radiation similar to normal, star-forming galaxies at the present day. In particular, we do not account for massive, population III stars that may have been prevalent at  $z \gtrsim 20$ . Tentative measurements of polarisation in the CMB by the WMAP satellite (Kogut et al. 2003) suggest that much of the IGM was ionised earlier than indicated by the SDSS quasars (e.g., Spergel et al. 2003). We explore the implications of this result in the context of our present model by allowing the escape fraction to evolve with redshift. In the future, we will explore the combined effect of reionisation by both population II and population III stars.

In the next section we review some of the technical aspects related to our method, including the approximations inherent to our radiative transfer calculations. We then follow with a description of the cosmological simulation that will be used in our analysis. Next, we discuss our methodology for source selection and present an in-depth analysis regarding resolution effects and how to correct for them. Finally, we discuss the results of our reionisation simulation and review the properties of the inhomogeneously ionised IGM and make comparisons with observational constraints.

## 2. SIMULATING COSMOLOGICAL REIONISATION

In general, a description of the evolution of ionised regions around cosmological sources requires a full solution to the radiative transfer equation. Such a solution would yield everywhere the monochromatic specific intensity of the radiation field in an expanding universe:  $I_\nu \equiv I(t, \vec{x}, \hat{n}, \nu)$ , where  $\hat{n}$  is a unit vector along the direction of the propagation of a ray with frequency  $\nu$ . Presently, it is computationally impractical to obtain a complete, multi-dimensional solution for  $I_\nu$  at the high resolution required for cosmological simulations. Our approach relies on an algorithm which approximates the full solution from ionising sources by semi-independently processing the net effect of each source separately (see Sokasian et al. 2001). Owing to the large number of sources and the fact that the order in which sources are processed is randomised at each step, the departure from the fully self-consistent solution is negligible. (We have verified this explicitly by running different cases in which the ordering of the sources varies and shown that our results are unaffected.) By adopting this approximation, we are able to employ a simple jump condition to compute all radiative ionisations from a given source in a single step. This eliminates the need to repeatedly re-cast rays and calculate rates at every time step, thereby greatly speeding up the analysis. Ionisation fractions within ionised regions are then computed by assuming photoionisation equilibrium.

To further speed up the calculations, the ray casting scheme used in Sokasian et al. (2001) has been modified to incorporate an adaptive scheme based on the method described by Abel & Wandelt (2002). In particular, the transfer of direct source photons is computed on a uniform Cartesian grid by casting a set of base rays which subsequently split hierarchically according to a local refinement criterion which involves keeping the ratio of the area of a cell to the area associated with the ray on a given hierarchical level above a fixed threshold value. This criterion ensures that a minimum number of rays pass through any given cell. The underlying pixelisation scheme that governs how rays are split has the property of exactly tiling a sphere with equal areas, ensuring equal photon flux per ray for isotropic sources. Rays are propagated until they travel at most  $\sqrt{3}$  times the box length (assuming periodic boundary conditions) or the assigned number of photons is exhausted. Once the ionisation level in the simulation box has reached significant levels, periodic boundary conditions are turned off and photons reaching the edges are added to a pool associated with the diffuse background. At the end of each interval, the effect of a diffuse ionising background is accounted for by casting rays of ionising radiation (according to a detailed prescription) inward from the sides of the simulation box. Density fields, clumping factors and information regarding sources is specified from outputs at desired redshifts from the underlying cosmological simulation (see Sokasian et al. 2001 for technical details).

Our approach entails a number of straightforward approximations to simplify the calculations; we summarise them briefly here. First, our radiative transfer calculations are done on a uniform grid whose scale  $L$  will always be much smaller than the horizon,  $c/H(t)$ , where  $c$  is the speed of light and  $H(t)$  is the time dependent Hubble constant. This eliminates the need to include Doppler shifting of frequencies in line transfer calculations. Additionally, if the light crossing time,  $L/c$ , is much shorter than the ionisation timescale, the time dependence of the intensities drops out as well. In the volumes we simulate, this will certainly be true and so we make this approximation. Next, we assume that the density field will experience negligible cosmological evolution during a single timestep. This assumption allows us to perform all our radiative calculations during a given timestep in a static density field, greatly reducing the complexity of the algorithm. In our analysis we find that a constant time step of  $4.0 \times 10^7$  yr satisfies the latter assumption and manages to capture the characteristic timescale over which source intensities change. Moreover, we find that the chosen timestep allows us to reliably track the morphological evolution of the reionisation process during early epochs when the rate of sources switching on is relatively fast.

Finally, we ignore the dynamical consequences of thermal feedback into the gas from radiative ionisation, enabling us to decouple our calculation of the radiation field from the hydrodynamical evolution of the gas. This allows us to use existing outputs from cosmological simulations to describe the evolving density field during the reionisation process. In reality, photoheating introduces extra thermal energy into the medium, and as ionisation fronts (I-fronts) move from small scales to large scales, there is a corresponding transfer of power from small to large scales through nonlinear evolution. This effect is somewhat accounted for in the underlying cosmological simulation used in this paper which includes a uniform ionising background capable of heating the gas. However, one also expects additional heating due to radiative transfer effects during the reionisation process, and such uniform backgrounds cannot reproduce the observed increase in gas temperatures from the extra heating (Abel & Haehnelt 1999 and references therein). As a result, we expect minor systematic errors to be present in our solutions. However, the main purpose of this paper is to describe the general morphological evolution of the reionisation process on large scales, which is insensitive to these systematic errors. In particular, recombination rates depend weakly on temperature and hence a proper accounting of photons is possible even if the temperatures are not computed precisely.

## 2.1. Treating Multi-Species Reionisation

One of the models we consider in this paper includes sources which are capable of ionising both hydrogen and helium simultaneously. In this case, it becomes necessary to couple the corresponding ionisation fractions during the radiative transfer calculations. Exact solutions require taking into account the detailed frequency dependences of all the relevant processes and solving the multi-species chemical reaction flows in nonequilibrium (e.g. Anninos et al. 1997). Owing to the large number of sources which need to be processed in our study, the implementation of a fully consistent nonequilibrium chemistry solver would require computations that are not presently feasible. Fortunately, there are a number of simplifying approximations which we are able to employ that greatly speed up the calculations without compromising the main objectives of our study.

Our analysis of hydrogen and helium reionisation requires us to track three ionisation zones: H II, He II, and He III. In order to simplify our calculations, we decouple the ionisation calculations by applying separate ray tracing calculations for each species. To properly account for the recombination rates implicit in the radiative transfer calculations, we are required to follow a particular ordering for the ray tracing. Specifically, since He III ionisation zones will always reside within H II zones, we first apply ray tracing calculations for He II reionisation which incorporate recombination rates based on electron densities that assume complete ionisation in both hydrogen and helium. Although the equations for H I and He II ionisation are, in principle, coupled, they can be separated to good accuracy using the fact that recombination processes from He III to He II are able to ionise H I. In particular, recombination emission from He II  $L\alpha$  ( $h\nu = 40.7$  eV) photons, which diffuse slowly owing to resonance scattering, and He II Balmer-continuum photons, which are concentrated close to the H I ionisation threshold, will tend to ionise H I within the He III zone. For near cosmic abundances, these two processes are just about sufficient to balance H II recombination within this zone (e.g. Osterbrock 1989). An additional source of H I ionising radiation produced in this zone is He II two-photon continuum emission for which  $h\nu' + h\nu'' = 40.7$  eV (the spectrum peaks at 20.4 eV). Most of these photons are able to escape out of the He III zone and should, in principle, be added to the pool of photons which will be responsible for ionising the H I zone. In order to access the maximal contribution from this process relative to the contribution already present from the stellar radiation field, we examine the hypothetical scenario where the IGM is completely doubly ionised in helium by  $z = 10$ . Assuming a gas temperature of  $2 \times 10^4$  K and a gas clumping factor of 30, we estimate that the total contribution of ionising photons from He II two-photon emission will comprise only 1% of the total number of photons produced directly from star-forming galaxies at the same redshift. Given the fact that the uncertainties associated with intrinsic source intensities are larger, we ignore this additional



component to simplify the calculations.

Once the He III zone has been determined, the next step involves calculating the associated H II and He II zones around the same source. Here we note that the stellar radiation field responsible for ionising the latter two species can only arise from the hottest OB stars in the galaxies. This assumption is based on the fact that only these stars have strong enough stellar winds capable of producing *escape routes* through the host galaxy for their ionising radiation. Since the intrinsic spectra of OB stars yield a large fraction of photons with  $h\nu > 24.6$  eV, the outer boundaries of the ionisation zones for H II and He II coincide, thereby allowing the tracking of both zones via a single ray tracing calculation. The approximation here will be to track H II ionisations explicitly via ray tracing while implicitly assuming that He II is ionised to the same degree and extent. Since the relative cosmic abundance of helium is small ( $\sim 8\%$  by number density), the inaccuracies introduced by this approximation should be negligible. Note that in carrying out the radiative transfer calculations for the ionisation of H I, we are careful to ignore H II recombinations within the He III regions for the reasons presented earlier.

After the ionisation zones have been determined, ionisation fractions for He III and H II are calculated by applying the following equilibrium condition for each case,

$$C_f n_e n_+ \alpha_A(T) = \Gamma n_o, \quad (1)$$

where  $C_f$  is the volume averaged gas clumping factor within the cell,  $\alpha_A(T)$  is the temperature dependent Case A recombination coefficient, and  $n_+$ ,  $n_o$ , and  $n_e$  are the ionised, neutral, and electron number densities, respectively. In this paper, we assume a constant temperature of  $2.0 \times 10^4$  K for all regions which have undergone ionisation to He III and  $5.0 \times 10^3$  K for regions having undergone ionisation to H II and He II only, (see Abel and Haehnelt 1999). This allows us to simplify our calculations by using constant recombination coefficients. From the fitting formulae given in Hui & Gnedin (1997), we compute the relevant coefficients to be  $\alpha_{A,\text{HeIII}} = 1.40 \times 10^{-12} \text{ cm}^3 \text{ s}^{-1}$  and  $\alpha_{A,\text{HII}} = 2.59 \times 10^{-13} \text{ cm}^3 \text{ s}^{-1}$  for  $T = 2.0 \times 10^4$  K and  $\alpha_{A,\text{HI}} = 6.98 \times 10^{-13} \text{ cm}^3 \text{ s}^{-1}$  for  $T = 5.0 \times 10^3$  K. The photoionisation rate in an ionised cell for a given species will be approximated by

$$\Gamma = \frac{\bar{\sigma} \dot{N}_{ph}}{4\pi r^2} \text{ s}^{-1}, \quad (2)$$

where  $\bar{\sigma}$  is the mean cross section for photoionisation,  $\dot{N}_{ph}$  is the number of relevant ionising photons released per second from the source, and  $r$  is the distance from the source to the cell in question. Assuming that the sources have intrinsic spectral energy distributions of the form  $J(\nu) \propto \nu^{-\alpha}$  in the relevant frequency range of interest and that  $\sigma(\nu) \propto \nu^{-3}$  beyond the ionisation edge, we can approximate the mean photoionisation cross sections according

to

$$\bar{\sigma} = \sigma_o \frac{\alpha}{\alpha + 3}, \quad (3)$$

where  $\sigma_o$  is the cross section at the ionisation frequency. For stellar sources we choose  $\alpha = 1.8$  (up to 4 Ryd) based on the extrapolated far-UV synthetic spectrum for starburst galaxies derived in Haehnelt et al. (2001). Interestingly, this value is also consistent with estimates for the average quasar spectral index (see the relevant discussion in Sokasian et al. 2002), simplifying our analysis involving reionisation by harder sources such as AGNs (see §5.4). In this paper we adopt  $\sigma_{\text{HeII},o} = 1.58 \times 10^{-18} \text{ cm}^2$  and  $\sigma_{\text{HI},o} = 6.30 \times 10^{-18} \text{ cm}^2$  from Osterbrock (1989).

To further simplify our calculations, we remove the coupling between the ionisation fractions of the two species by approximating separate expressions for the electron densities in each ionisation zone. Specifically, ionisation fractions for He III are computed first by approximating the medium within the He III as fully ionised in He II and H I, thus giving

$$n_e = (\chi_{\text{HeIII}} + 1)n_{\text{He,tot}} + n_{\text{H,tot}}, \quad (4)$$

where  $n_{\text{H,tot}}$  and  $n_{\text{He,tot}}$  represent the total hydrogen and helium particle densities, and  $\chi_{\text{HeIII}}$  is the ionisation fraction for He III. Ionisation fractions for H II are then computed using

$$n_e = (\chi_{\text{HeIII}} + \chi_{\text{HII}})n_{\text{He,tot}} + \chi_{\text{HII}}n_{\text{H,tot}}, \quad (5)$$

where we have approximated  $\chi_{\text{HeII}} = \chi_{\text{HII}}$  based on our earlier assumptions related to the nature of the sources responsible for ionising hydrogen and singly ionising helium. Again, since the helium abundance is small the latter approximation should be relatively accurate. Although our procedure for calculating ionisation fractions is not fully consistent, the resultant inaccuracies are relatively small and certainly fall within the broader uncertainties associated with the simulation as a whole.

The approximations listed above offer computational benefits that allow us to process a large number of sources easily. Since they do not compromise the main objective of this paper, which is to study the morphological evolution of reionisation, we feel justified in adopting them.

### 3. UNDERLYING COSMOLOGICAL SIMULATION

The cosmological simulation we will use in our analysis is based on a SPH treatment of a  $\Lambda$ CDM model with parameters  $\Omega_o = 0.3$ ,  $\Omega_\Lambda = 0.7$ , Hubble constant  $H_o = 100 h$

km s<sup>-1</sup> Mpc<sup>-1</sup> with  $h = 0.7$ , baryon density  $\Omega_b = 0.04$ , and a scale-invariant primordial power spectrum with index  $n=1$ , normalised to the abundance of rich galaxy clusters at the present day ( $\sigma_8 = 0.9$ ). These choices are in good agreement with those inferred from the WMAP observations (Bennett et al. 2003).

The simulation uses  $324^3$  SPH particles and  $324^3$  dark matter particles in a  $10.0 h^{-1}$  Mpc comoving box, resulting in mass resolutions of  $2.12 \times 10^6 h^{-1} M_\odot$  and  $3.26 \times 10^5 h^{-1} M_\odot$  in the dark matter and gas components, respectively. This particular simulation represents one of the high-resolution runs (simulation Q5) in the series of calculations performed by Springel & Hernquist (2003a). These authors used a large set of high-resolution simulations on interlocking scales and at interlocking redshifts to infer the evolution of cosmic star formation from high redshift to the present. These simulations included a novel description for star formation and feedback processes within the interstellar medium and a treatment of galactic outflows (Springel & Hernquist, 2003b), and employed a conservative formulation of SPH based on following the specific entropy as independent thermodynamic variable (Springel & Hernquist, 2002). The broad range of scales encompassed by their set of simulations, together with extensive convergence tests, enabled them to obtain a converged prediction for the cosmic star formation rate,  $\dot{\rho}_*$ , within the adopted model for galaxy formation.

In the following section we will discuss the motivation behind our particular choice for the simulation scale. We will also describe our methodology for selecting sources and assigning intensities in the context of the converged prediction for  $\dot{\rho}_*$  from Springel & Hernquist (2003a).

#### 4. SOURCE SELECTION

To accurately simulate the reionisation process due to stellar sources, one requires the cosmological volume to be sufficiently large to properly sample a representative range of halo masses. At the same time, one is inhibited from adopting an excessively large volume which can compromise the technical feasibility of the simulation owing to the large number of sources which would need to be processed. Furthermore, one requires sufficient mass resolution within the simulated volume in order to reliably measure star formation rates in galaxies. This is especially true at high redshifts, where the bulk of the star formation occurs in objects of relatively low mass, as expected for hierarchical growth of structure, making it important to resolve low-mass objects. From the set of simulation runs presented in Springel & Hernquist (2003a), we find that their Q5 run provides the most appropriate compromise ( $10.0 h^{-1}$  Mpc box length), capable of capturing a representative sample of

the halo population while maintaining a level of mass resolution that reliably matches the converged star formation rate.

#### 4.1. Source Definition

Our approach for defining sources relies on identifying virialised halos as sites of star formation. As in Springel & Hernquist (2003a), halos are located by employing a “friends-of-friends” (FOF) group finder algorithm to the dark matter particles. The algorithm is restricted to dark matter particles only to avoid complications associated with tracking baryonic particles whose number and type can vary with time. The two main parameters which govern the group-finding algorithm are the comoving linking length and the minimum number of particles required for a group. For the former, we choose a fixed value equal to 0.2 times the mean interparticle spacing of dark matter particles, corresponding to a group overdensity of roughly 200. The choice for the minimum number of particles which can define a group is somewhat more arbitrary. This is due to the fact that this parameter is invariably related to the question as to what exactly constitutes a group. A reasonable definition may be that given a specific overdensity, a group is considered to be *real* if it can be reliably tracked over time. More specifically, this would correspond to being able to find a given halo in a subsequent time step. Below a certain threshold, one might start to identify *transient* groups, that dissolve away in subsequent time steps. Our statistics on halo tracking indicate that this threshold is around 100 dark matter particles, with associated uncertainty growing progressively towards lower particle numbers; i.e. below about 100 particles one starts to occasionally pick up transient halos that are probably flukes, and the fraction of these slowly grows towards smaller groups. However, as we shall show in the following section, a significant portion of the total star formation rate is predicted to come from low-mass halos with fewer than 100 dark matter particles. These objects essentially represent the star-forming mini-halos of the Universe. In order to account for these sources, we adopt an aggressively low minimum value of 16 particles for our definition of a group. This will inevitably raise the level of uncertainty regarding the reality of some of the low-mass halos and their corresponding star formation rates. However, this approach provides us with a list of low-mass objects whose number density and spatial locations are statistically consistent with results from simulations conducted with higher resolution. The star formation rates in these objects can then be systematically corrected so that the total contribution from all objects matches the converged result presented in Springel & Hernquist (2003a).

## 4.2. Star Formation Rates

Our prescription for assigning star formation rates to the groups relies first on associating each gas or star particle with its nearest dark matter particle, and the FOF-group this particle resides in. We then take the total mass of each group as a “viral” mass, and the sum of star formation rates in all of a group’s SPH particles as the total star formation rate in the halo. Our working assumption will then be that every halo hosts a single galaxy which will act as a source. In reality, however, there may be more than one galaxy per halo. The difference, however, is negligible in the context of the spatial resolution of the radiative transfer calculations. More specifically, in the redshift range of interest, even the most massive halos have virial radii which are less than or comparable to the width of a single cell.

In Figure 1, we plot various statistical quantities related to the star formation rate from the resultant source list as a function of halo mass for redshifts  $z = 14.7, 10.4,$  and  $7.2$ . At each redshift we have binned the halos by mass in logarithmic intervals of  $d\log M = 0.1$  and computed the associated star formation rate density, number density, fractional star formation contribution, and cumulative star formation contribution below a given mass. From the first two rows of plots, it is evident that while the relative amplitude in the star formation rate becomes smaller towards the lower mass scales, the number of halos rises dramatically. Note also the overall rise of the star formation rate with decreasing redshift. In Hernquist & Springel (2003), the authors used simple analytic reasoning to identify the physical processes that govern this evolution. As part of their conclusions, they find that at early times ( $z > 6$ ), densities are sufficiently high and cooling times are sufficiently short that abundant star-forming gas exists in all dark matter halos with  $T_{\text{vir}} > 10^4$  K that can cool by atomic line cooling. Consequently, the evolution of the star formation rate is dominated by gravitationally driven growth of the halo mass function, as is seen here. The relative contribution to the total cosmic star formation rate density as a function of halo mass is shown in the bottom two rows of Figure 1. Here we see that intermediate mass scales provide the largest contribution to the overall total, with a progressively larger contribution from higher mass scales at decreasing redshifts.

Owing to the finite dynamic range of the cosmological simulation, we cannot expect to resolve *all* the star forming halos that contribute to the ionising emissivity. This becomes progressively problematic at high redshifts where most of the star formation takes place in low-mass galaxies which form in abundant numbers as progenitors of more massive systems. Furthermore, near the resolution limit of identifiable halos, the corresponding star formation rate becomes less reliable owing to the relatively small number of SPH particles associated with the halo. The resultant star formation missed by our simulation due to

these resolution effects is shown in Figure 2 for the redshift range of interest. In the top panel we plot the total star formation rate from all the halos identified in our simulation (dashed line) and compare it to the physically motivated analytic fit to numerical converged results presented in Springel & Hernquist (2003a). The analytic fit, obtained from the analysis of Hernquist & Springel (2003), takes the form of

$$\dot{\rho}_\star = \dot{\rho}_\star(0) \frac{\chi^2}{1 + \alpha(\chi - 1)^3 \exp(\beta\chi^{7/4})}, \quad (6)$$

where,

$$\chi(z) = \left( \frac{H(z)}{H_o} \right)^{2/3}, \quad (7)$$

and  $\alpha = 0.012$ ,  $\beta = 0.041$ , and  $\dot{\rho}_\star = 0.013 \text{ M}_\odot \text{ yr}^{-1} \text{ Mpc}^{-1}$  define the fitting parameters. The above fitting function was motivated by the bimodal behaviour in the evolution of the cosmic star formation rate. At low redshifts, the efficiency of gas cooling processes is diminished owing to the expansion of the Universe and hence manifests itself through a scaling that is related to the expansion rate as quantified by the Hubble constant. At high redshifts, the steep rise towards lower redshifts is related to the growth of the halo mass function which exhibits an exponential cut-off for large masses. To assess the significance of the discrepancy between the numerical and the theoretical results in the context of the reionisation of the Universe, we find it convenient to relate star formation rates in terms of the cumulative number of ionising photons released as a function of look-back time. In the bottom panel of Figure 2 we plot this quantity in terms of a ratio between the simulation results and the theoretical prediction. Here we have adopted a conversion factor of  $10^{53} \text{ s}^{-1}$  ionising photons per star forming rate of  $1 \text{ M}_\odot \text{ yr}^{-1}$  based in the analysis from Madau et al. (1999). We find that in terms of the cumulative number of ionising photons released, the discrepancy does not become dramatic until one exceeds a redshift of  $\sim 15$  or so.

#### 4.2.1. Correcting Star Formation Rates in Low-Mass Sources

The discrepancy described above does not pose a serious obstacle in the context of our present goals; we find that we can easily correct for the missing star formation rate through a simple algorithm by adjusting the rates in the low-mass halos.

We start first by deciding upon a mass threshold for halos above which we are confident in our results for the associated star formation rate. After analysing the results from the group finding algorithm applied to our simulation, we find that independent of redshift,

halos with masses  $M > 3.0 \times 10^8 h^{-1} M_\odot$  have statistically reliable values for their star formation rates. Below this threshold, a halo may simply not have enough SPH particles to make it possible to reliably compute the star formation rate or the halo may be unresolved altogether. The fact that our source list aggressively includes low-mass objects allows us to partly compensate for the missing objects. Although the *reality* of some fraction of these low-mass objects may be questionable, the fact that the statistical properties regarding their number densities and locations matches those from higher resolution runs assures us that we can at least statistically capture the effect from this population of sources. By coupling the criterion regarding the *reality* of low-mass object with the criterion for confidence in the computed star formation rate, we can distinguish, in technical terms, two types of problematic sources: (1) objects whose *reality* is not questioned ( $n_{\text{DM}} > 100$ ), but whose star formation rate may be unreliable ( $M < 3.0 \times 10^8 h^{-1} M_\odot$ ), and (2) objects whose *reality* and corresponding star formation is questionable ( $n_{\text{DM}} < 100$  and  $M < 3.0 \times 10^8 h^{-1} M_\odot$ ). The net effect from both these sets of sources is to cause a deficit in the total cosmic star formation rate relative to the theoretical expectation. Our method for correcting this deficit involves supplementing all objects whose masses fall below  $3.0 \times 10^8 h^{-1} M_\odot$ , comprising both sets of problematic sources, with additional amounts of star formation in proportion to their mass. The total amount added to all these objects at a given redshift is normalised so that it exactly makes up the deficit relative to the theoretical prediction. In Figure 3 we plot the comoving number densities and the star formation rates as a function of redshift for all the sources in the simulation. In the context of the deficit in the cosmic star formation rate, we have grouped the sources into three categories with the first column representing sources which do not require any corrections and the second and third columns including the aforementioned problematic sources. Here the dashed line and solid line indicate the uncorrected and subsequently corrected contribution to the total star formation rate, respectively. It is evident from the plots that the corrections to the low-mass sources do not appear to be drastic and we are confident that the uncertainties related to these adjustments cannot significantly affect our results.

Having adjusted star formation rates in the low-mass sources we can now estimate the magnitude of the discrepancies in the total star formation rate had we been limited to poorer mass resolutions. In Figure 4 (*left panel*) we plot this discrepancy in terms of the fraction of the total star formation contributed from sources with halo masses above a certain mass. The total star formation rate is based on all halos above the resolution limit in our simulation ( $M = 3.9 \times 10^7 h^{-1} M_\odot$ ). In the same figure (*right panel*) we also plot source number densities as a function of redshift for the same mass ranges, with the total source density from the simulation also shown (*solid line*). As in Figure 1, it is evident that the subsequent fraction of star formation contributed by relatively low-mass

objects rises rapidly with redshift. The labeled mass inequalities were chosen to roughly match the source mass resolutions associated with recent numerical attempts to simulate IGM reionisation by stellar sources (see Ciardi et al. 2003b and Razoumov et al. 2002). Interestingly, we find that in the context of our corrected source list, the quoted mass limits continue to significantly underestimate the relative contribution to the total star formation rate from low-mass objects even at intermediate redshifts when the ionising emissivity in the IGM is expected to have reached appreciable levels. In particular, at  $z \simeq 9.2$  the cases with  $M > 1.0 \times 10^9 h^{-1} M_{\odot}$  and  $M > 0.3 \times 10^9 h^{-1} M_{\odot}$ , which are close to the mass resolution of sources in the 'M3' and 'S3' simulations described by Ciardi et al. (2003b), appear to account for only  $\simeq 53\%$  and  $\simeq 81\%$  of the total star formation rate, respectively, relative to our complete source list. It is of course possible to renormalise the star formation rates in the massive (resolved) sources so that the total star formation rate is corrected to agree with our converged results. However, such a simple correction fails to address the potentially significant impact the environments around sources can have on the amount of ionising radiation that can escape into the IGM. In particular, by concentrating the ionising flux away from low mass system which are more likely to reside in less clumpy environments than their more massive counterparts, one runs the risk of systematically overestimating recombination rates. We will explore the ramifications from such corrections in context of our own results in §5.1.

### 4.3. Source Gridding

Given the redshift range of interest,  $6 \lesssim z \lesssim 20$ , and our time step for updating source lists,  $\Delta t = 4.0 \times 10^7$  yrs, the total number of sources which require processing reaches nearly  $1.5 \times 10^5$ . Since our radiative transfer calculations are performed on a Cartesian grid with a limiting resolution, it is logical to group together sources within cells as a method of reducing the number of sources. Owing to the high resolution of our grid (200<sup>3</sup>), the overall number of sources is reduced only by 2%. Such a marginal reduction in sources assures us that the resolution of our grid provides excellent resolving power in regards to the spatial distribution of the sources.

## 5. RESULTS AND DISCUSSION

In our analysis, we carefully follow the reionisation process from a set of models parameterised by the escape fraction. In this context, the escape fraction is defined to be the fraction of ionising photons intrinsic to each source that escape and enter into



the radiative transfer calculations. It must be noted here that this parameter inevitably also carries with it any uncertainties associated with the underlying amplitude of the star formation rates computed for the sources. Nevertheless, our approach allows us to predict the epoch of reionisation as a function of this parameter. By comparing these predictions with recent observational constraints on the escape fractions and neutral densities near  $z \sim 6$ , we are able to test the overall consistency of the theoretical predictions of the computed star formation rates. Along the way we are also able to make general statements regarding the morphological aspects of reionisation.

### 5.1. Global Ionisation Fractions

The evolution of the global ionisation fraction in the simulation volume provides a useful way of characterising the overall ionisation state of the Universe as a function of redshift. In Figures 5a and 5b we show how the ionised mass-weighted and volume-weighted fraction, respectively, evolve with redshift. The rate of the evolution to a completely ionised state is quite similar for all the models, although there is a subtle trend towards a swaller rise of ionisation fractions with decreasing escape fractions. Nevertheless, in all cases the reionisation epoch, which we define as the redshift when the global volume-weighted ionisation fraction reaches 99%, occurs by  $z \sim 7$ . Later in this section we show how a more detailed analysis involving statistical comparisons between simulated spectra and observational results for flux transmission at  $z \simeq 6$  can lead to more rigid constraints as to how early reionisation could have taken place.

Figures 5a and 5b also show that the ionised mass-weighted fraction is consistently larger than the volume-weighted fraction at redshifts before reionisation. This result is seen more clearly in Figure 5c where we have plotted the corresponding ratio of the two fractions. The larger values for the ionised mass-weighted fraction at early redshifts is consistent with the general picture of the pre-overlap epoch where sources are preferentially ionising their relatively dense surroundings before affecting the more tenuous IGM. The fact that the inequality between the mass and volume fraction is amplified with decreasing escape fraction highlights an interesting morphological feature related to the number and intensity of the sources responsible for reionisation. Namely, when escape fractions are low, a relatively larger number of sources are directly involved in the process of ionising a neutral density field. Since the ionisation zones associated with these sources are also smaller, the net effect is that massive regions are more likely to be ionised from the ionising radiation emanating from within rather than radiation that has first traversed the less dense IGM. This predilection naturally manifests itself in relatively larger ratios for the mass-to-volume

ionisation fractions during the early stages of reionisation in these cases. Eventually, intervening patches of neutral material become ionised and there is a sharp rise in the intensity of the ionising background as contributions from different sources combine. As this diffuse component comes to dominate the radiation field, all regions become uniformly ionised and the ratio of mass-to-volume ionisation fraction converges to unity.

A visual illustration of the reionisation process is shown in Figure 6 where we plot a series of projected slices through the simulation volume. In each panel, a  $0.25h^{-1}\text{Mpc}$  slice from the  $f_{esc} = 0.10$  run is projected in both density and ionisation fraction. Source locations in each slice are denoted by white crosses making it easier to follow how the ionised regions (*blue*) percolate to turn a neutral IGM (*yellow*) into one that is highly ionised (*red*). Compared with earlier studies of reionisation, Figure 6 shows that morphologically the ionised regions in our analysis trace the large scale distribution of sources. In particular, we do not find that reionisation occurs mainly from low- to high-density regions, as would be the case if photons escaped preferentially into the IGM before ionising the high density regions near the sources.

The panels in Figure 6 graphically illustrate the large number of sources that are involved in the highly inhomogeneous reionisation process. A more dramatic illustration of this point is shown in Figure 7 where we have plotted a 3D image of the same simulation showing iso-surfaces around the ionised regions at  $z = 12.08$ . This highly inhomogeneous morphology represents a departure from the general picture of reionisation proposed by Gnedin (2000) where only a handful of bright sources are responsible for reionising the Universe. In the following section we discuss how the morphology of the reionisation process can affect the number of ionising photons required to achieve full reionisation.

## 5.2. Ionising Photon Budget

The number of ionising photons per hydrogen atom required for the ionised regions around sources to completely overlap has developed into an interesting topic that is commonly addressed in studies of this kind (Ciardi et al. 2003b, Razoumov et al. 2002, Haiman et al. 2001, Miralda-Escudé et al. 2000, Gnedin 2000). To reliably estimate this quantity with simulations requires a high level of resolution capable of properly estimating gas clumping factors which govern the overall recombination rate. This requirement is especially important in light of the results presented in Haiman et al. (2001) which show that mini-halos with temperatures below  $\sim 10^4\text{K}$  can dominate the average clumping in the early stages of reionisation and significantly increase the required photon budget necessary to achieve complete overlap. Given the high resolution inherent to our hydrodynamic

simulations and the corresponding radiative transfer grids, coupled with our ability to probe clumping factors on sub-cell scales based on the underlying distribution of SPH particles, we are able for the first time to probe the scales needed to account for recombination effects arising from such low-mass objects. This represents a significant improvement upon previous attempts which have relied on conservative assumptions related to the escape fraction to accommodate unresolved clumping.

In Figure 8, we plot the cumulative number of escaping ionising photons per hydrogen atom as a function of redshift. The diamond symbol on each curve corresponding to different values for  $f_{esc}$  represents the point at which the volume ionisation fraction exceeds 99%. For  $f_{esc} = 0.10 - 0.30$ , between 2 and 3 ionising photons are required to reionise the Universe while 4-5 ionising photons are needed in the case where  $f_{esc} = 1.0$ . The difference in the number of required ionising photons resulting from variations in the escape fraction arises from the interesting interplay between the evolution of clumping factors and the mean density of the Universe. In particular, the rapid evolution of the mean density plays a slightly more important role than the evolution of clumping factors in the redshift range of interest. Therefore, a delay in reionisation to lower redshifts requires fewer ionising photons since the decline in gas densities outweighs the corresponding increase in clumping factors, resulting in comparatively fewer recombinations occurring than at higher redshifts.

Environmental factors influence the number of photons required to produce reionisation. A related issue is whether the distribution of ionising intensities among the sources themselves can also have an important impact on this process. In particular, given the same amplitude and evolution of the cosmic star formation rate, it is interesting to explore how a redistribution of the ionising flux from dim low-mass sources to more massive sources would affect reionisation. In Figure 9, we examine this scenario by way of comparisons involving the volume-weighted ionisation fraction and the cumulative number of ionising photons that are released. Specifically, we examine two situations: 1) the case where we have retained the full source list which includes sources down to our resolution limit of  $M \simeq 3.9 \times 10^7 h^{-1} M_{\odot}$ , and 2) the case where we have systematically transferred ionising fluxes from sources with  $M < 1.0 \times 10^9 h^{-1} M_{\odot}$  to the nearest neighbouring sources with masses above this limit. The figure shows that the affect can be significant, namely that reionisation takes place later and requires more photons (by roughly  $\simeq 63\%$ ) for the same escape fraction ( $f_{esc} = 0.20$ ) when low-mass sources are excluded. This result stems from the fact that low-mass sources preferentially reside in less clumpy environments than their massive counterparts. Consequently, the net effect of transferring ionising flux from these sources to more massive systems amounts to increasing the overall ionising intensity in regions with higher recombination rates. This leads to recombinations playing a more dominant role and thus delaying the onset of reionisation. This finding therefore supports

the requirement that dim low-mass sources be properly resolved and included in future simulations of this kind. In particular, inaccuracies related to the inability to resolve low-mass sources and their corresponding contribution to the cosmic star formation rate may be amplified due to their preferential location in less clumpy environments.

### 5.3. Observational Comparisons: *Flux Transmittance*

Recent discoveries of quasars at redshifts 5.8 and greater (Becker et al. 2001, Fan et al. 2001, Fan et al. 2000) are finally making possible quantitative studies of the status of the IGM at high redshifts. In Fan et al. (2000) the spectrum of a  $z = 5.8$  quasar (SDSS J1010-0125) was examined and revealed no evidence for a Gunn-Peterson trough, indicating that the IGM was highly ionised near  $z \sim 5.5$ . In subsequent observations (Fan et al. 2001) the authors studied three new quasars at  $z > 5.8$  and found a significant increase in Ly $\alpha$  absorption from redshift 5.5 to 6.0. In particular, they found a  $\sim 300 \text{ \AA}$  region in the Ly $\alpha$  forest portion of the spectrum of a  $z = 6.28$  quasar (SDSS 1030.10+0524) which had a measured flux transmittance consistent with zero, indicating a flux decrement of  $\gtrsim 50$ , and suggesting the possible detection of a Gunn-Peterson trough. To more accurately quantify these findings Becker et al. (2001) obtained higher resolution spectra of the three new  $z > 5.8$  quasars, allowing them to place better constraints on the status of the high redshift IGM.

To relate our results to these observations, we extract artificial Ly $\alpha$  absorption spectra from the simulation outputs and then derive statistical probabilities for the resultant flux transmittance which can readily be compared to the observational results. We extract artificial spectra using the particle information in the SPH simulation coupled with the ionisation information from our radiative transfer calculations. For each model, we generate 500 spectra along randomly selected lines of sight (LOSs) between  $z \simeq 5.8 - 6.2$ . Our procedure is similar to that in the TIPSYS software package (Katz & Quinn 1995), but does not require that a LOS be perpendicular to a box face in the simulation volume. Each LOS has a unique and arbitrary direction relative to the box coordinate system and wraps through the simulation volume repeatedly via periodic boundaries. Using the smoothing kernels of the SPH particles, gas densities and temperatures are computed along a LOS at appropriately sampled intervals. The component of the peculiar velocity of the gas in the direction of the LOS is also computed at each point. Once all physical quantities have been gathered, Voigt profiles are fitted to each spectrum by interpolating between the corresponding line-absorption coefficients provided in Harris (1948). It is important to point out that in computing the line profiles we use a minimum gas temperature of  $5.0 \times 10^3$

K as a correction to the SPH temperatures which exclude the extra heating introduced by radiative transfer effects (see Abel and Haehnelt, 1999).

Our simulations were stopped at  $z = 5.8$ , allowing us to make comparisons with the observational results from the spectrum of the  $z = 6.28$  quasar. The presence of an apparent Gunn-Peterson trough in the spectrum of this quasar makes it an especially interesting case. By using the results of our simulated spectra to make statistical comparisons with this region and another region with a non-zero transmittance, we can constrain the evolution of the reionisation process. Our analysis is based on probability distribution functions involving transmission levels that have been averaged over the same redshift range as the observational measurements. Specifically, we focus on the redshift ranges  $5.95 < z < 6.16$  and  $5.74 < z < 5.95$ , corresponding to the regions over which the average transmittance was measured by Becker et al. (2001) in the spectrum of the  $z = 6.28$  quasar. In Figure 10, we plot the probability distribution functions of simulated transmissions averaged over the two redshift ranges and overlay the corresponding  $\pm 1\sigma$  measurements from Becker et al. (2001) (*vertical-dashed lines*). The distributions were obtained using 500 LOS, although we have only plotted a restricted range of transmissions for the purposes of observational comparisons.

It is clear from Figure 10 that the ionising emissivities predicted in the models with  $f_{esc} = 0.10 - 0.20$  provide the most plausible match to the observational results in terms of transmission probabilities for the two redshift ranges. For this choice, reionisation is expected to have occurred near  $z \simeq 7.8$ , although as the analysis here demonstrates, the IGM remains fairly opaque until  $z \sim 6$ . This spread in redshift between the time when the Universe first became ionised and the time when opacities declined enough to allow non-zero transmission in Ly $\alpha$  is important for the proper interpretation of observed quasar spectra. In particular, it is incorrect to assume that a volume-weighted ionisation fraction above 99% will necessarily produce non-zero transmission levels consistent with current observations of quasar spectra at  $z \simeq 6$ . A much more careful analysis involving extraction of spectra from simulations which include high precision information regarding ionisation fractions is necessary in order to make meaningful comparisons with observational results.

Interestingly, an escape fraction of 10 – 20% is reasonably close to the range of values ( $f_{esc} \lesssim 0.10$ ) that have been observationally deduced from  $z < 3$  starburst galaxies (see Heckman et al 2001; Hurwitz et al. 1997; Leitherer 1995). It is important to note that these observational results may be underestimating the true values of the escape fraction owing to undetected absorption from interstellar components. Also unclear, in context of our analysis, is the possible evolution of the escape fraction with redshift which may lead to significantly different values at  $z > 6$ . In any case, the fact that we require a reasonable

escape fraction in order to match the observations lends credence to the overall consistency of the theoretical predictions of the computed star formation rates.

#### 5.4. Hydrogen Reionisation By AGNs?

Our radiative transfer calculations have been designed to handle the simultaneous reionisation of both the hydrogen and helium components of the IGM. This allows us to explore the scenario where objects with spectra harder than stellar sources were primarily responsible for the reionisation of the Universe. Such a scenario has been proposed by e.g. Haiman & Loeb (1998). In their analysis, a theoretical extrapolation of the quasar luminosity function at fainter luminosities and higher redshifts than currently detected appears to favour reionisation by low-luminosity mini-quasars (or AGNs). Reionisation by AGN type sources has also been supported on the grounds that they may be the only type of sources capable of having large enough escape fractions to allow enough ionising photons to enter the IGM (see Wood & Loeb 2000).

To explore the implications of sources with hard spectra reionising the Universe, we have run a model in which the sources are capable of ionising He II in addition to H I. Specifically, He II ionising rates are computed for the sources by assuming a single power-law form for the spectrum,  $f_\nu \propto \nu^{-\alpha}$ , normalised to deliver the same number of H I ionising photons below 4 Ryd predicted from soft sources with  $f_{esc} = 0.20$ . This ensures that the hydrogen component of the IGM will reach roughly the same level of ionisation by  $z \sim 6$  as in the  $f_{esc} = 0.20$  stellar model and therefore will also provide a reasonable match to the observational results of Becker et al. (2001; see §5.3). Extrapolated results for the far-UV synthetic spectrum of a stellar population with continuous star formation reveals a typical quasar spectrum with  $f_\nu \propto \nu^{-1.8}$  up to 4 Ryd. Adopting the same spectral index above 4 Ryd for the hard sources allows us to relate the rate of ionising photons,  $\dot{N}_{ph}$ , in He II and H I directly with the expression

$$\dot{N}_p^{HI} h = \dot{N}_{ph}^{HeII} \left( \left( \frac{\nu_{HeII}}{\nu_{HI}} \right)^{-1.8} - 1 \right), \quad (8)$$

where  $(\nu_{HeII}/\nu_{HI})$  is the ratio of ionisation threshold frequencies for the two species. This leads to a conversion factor of  $\sim 0.08$  He II ionising photons for every H I ionising photon.

In Figure 11, we show the resultant evolution in the volume-weighted ionisation fraction for both soft and hard sources. Note how the hydrogen component in the IGM becomes reionised earlier in the case where hard sources are invoked. This is due to the fact that the He III regions now surrounding the sources act as an additional source of H I ionising

photons (see §2.1). The bottom panel of Figure 11 shows that the helium component becomes reionised by  $z \simeq 6.5$  in this case. Such an early reionisation epoch for helium by high redshift sources such as AGNs should be testable in the coming decade with the Next Generation Space Telescope. Nevertheless, an interesting question we can explore currently is whether such a scenario may also leave an imprint on He II ionisation levels at lower redshifts where observations currently exist. In particular, we would like to test whether a hypothetical population of AGNs which suddenly turn off at  $z = 5$  will have lingering effects in terms of subsequent ionisation levels when another known population of quasars turn on.

For such an analysis, we re-ran our most realistic quasar model (model 5) from Sokasian et al. (2002) with the initial conditions that the helium component in the IGM is doubly ionised everywhere in the box. We present the results showing the subsequent evolution in the volume-weighted ionisation fraction in Figure 12. Here the solid line represents the scenario described above while the dotted line indicates the original simulation where quasars turn on in a medium that is only singly ionised in helium. In the case where the IGM is initially fully ionised, we see that He III recombinations quickly cause the ionisation fraction to decrease shortly after  $z = 5$  when the ionising emissivity from quasars is still low. Eventually, the emissivity from quasars grows and the ionisation fraction starts to rise again. However by  $z \simeq 3$  enough recombinations have already taken place since  $z = 5$  to effectively remove all traces of an early reionisation epoch, leading to ionisation levels that are governed only by the quasar population. It thus appears as if the present observations cannot rule out the simple AGN scenario we have considered here.

### 5.5. Electron Optical Depth to the Surface of Last Scattering

The recent tentative measurement of polarisation in the CMB by the WMAP satellite (Kogut et al. 2003) suggests that reionisation occurred in a more complex manner than indicated by the SDSS quasars alone (e.g., Spergel et al. 2003). The measurements exhibit an excess in the CMB TE cross-section spectrum on large angular scales ( $\ell < 7$ ) yielding an electron optical depth to the CMB surface of last scattering of  $\tau_e = 0.17$ . The uncertainty associated with this measurement depends on fitting all parameters concerned with the TT power spectrum and the TE cross power spectrum. Kogut et al. (2003) obtain a 68% confidence range of  $0.13 < \tau_e < 0.21$  corresponding to an instantaneous reionisation epoch which occurred between  $14 < z < 20$ . None of the models we have considered in this paper is able reionise the Universe by such early redshifts.

The connection between the implications of the WMAP results and those of the SDSS quasars for the evolution of the IGM is unclear. In an attempt to determine the extent to

which the sources examined in this paper would require additional ionising emissivity to provide a consistent match with the WMAP measurements we consider an evolving escape fraction of the form  $f_{esc}(z) = 0.20e^{k(z-6)}$ . Here, a positive value for the parameter  $k$  has the effect of producing ionisation levels consistent with the observations from the  $z = 6.28$  SDSS quasar, as in the model with  $f_{esc} = 0.20$ , while leading to relatively larger ionising emissivities at higher redshifts. We note that with this choice for  $f_{esc}$ , the “escape fraction” can exceed unity. In the context of our present analysis, this simply means that the rate of production of ionising photons is higher than would be implied for our choice of the star formation history and the IMF. For simplicity, we absorb these uncertainties in what follows into our definition of the “escape fraction.”

In Figure 13 we compare three different cases for this form: 1) a case with a constant escape fraction of  $f_{esc} = 0.20$  ( $k = 0$ ; *solid-line*), 2) a case with  $k = 0.13$  resulting in an evolving escape fraction that rises to unity at  $z \simeq 18$  around when the first sources turn on (*dotted-line*), and 3) a case with  $k = 0.33$  resulting in an escape fraction that exceeds unity beyond  $z \gtrsim 11$  (*dashed-line*). In panels b and c of Figure 13 we plot the resultant evolution of the volume weighted H II ionisation fraction and the evolution of the electron optical depth to electron scattering,  $\tau_e$ , given by:

$$\tau_e(z) = \int_z^0 \sigma_T n_e(z') c \left| \frac{dt}{dz'} \right| dz', \quad (9)$$

where  $\sigma_T = 6.65 \times 10^{-25} \text{ cm}^2$  is the Thompson cross section and  $n_e(z')$  is the mean electron number density at  $z'$ . In the calculation of  $\tau_e$  we assume that helium is singly ionised to the same degree as the hydrogen component for  $z > 3$  and doubly ionised everywhere at  $z < 3$ .

It is evident from Figure 13 that matching the the optical depth measurement from WMAP with the sources studied here would require substantially larger ionising emissivities at high redshifts. In particular, only the case with  $k = 0.33$ , which reaches an escape fraction greater than 10 near  $z \simeq 18$ , is capable of producing the measured electron optical depth. Such a large increase in the stellar production rate of ionising photons would require either a greatly enhanced star formation rate at high  $z$  relative to that obtained by Hernquist & Springel (2003) or an IMF which becomes more top-heavy with increasing redshift, as might be expected for population III type stars. In a recent paper Ciardi et al. (2003a) argue that a separate population is not necessary if one adopts a top-heavy IMF for population II type stars with an optimistically large value for the escape fraction. However, it is unclear whether the escape fraction adopted in their analysis is meaningful because of their inability to resolve either clumping on sub-grid scales or objects below  $10^9 M_\odot$ . Furthermore, in their best-fit model, reionisation is complete by  $z \simeq 13$ . Such an early reionisation seems difficult to reconcile with observations of the Gunn-Peterson effect



measured in the  $z = 6.28$  SDSS quasar (Becker et al 2001).

## 6. CONCLUSION

We have utilised a fast radiative transfer code to study the reionisation of the Universe by stellar sources. Our method has been applied to a high resolution cosmological hydrodynamical simulation which enables us to probe scales previously unresolved in similar type of studies. By supplementing a *one-step* radiative transfer code specifically designed for ionisation processes with an adaptive ray-tracing algorithm, we are able to significantly speed up the calculations and are able to handle a large number sources.

One of the main goals of this analysis was to study the effect of low-mass sources residing in mini-halos on the overall morphology of the reionisation process. Analysis of numerically converged results for star formation rates and halo mass functions in the underlying cosmological simulation allowed us to assess the resolution effects associated with low-mass objects and apply well motivated corrections. With these corrections, we were able to reduce the effective mass resolution limit for source objects to  $M \sim 4.0 \times 10^7 h^{-1} M_{\odot}$ , which is roughly an order of magnitude smaller than previous studies of this kind. Our calculations reveal that the process by which ionised regions in the IGM percolate is highly inhomogeneous and especially sensitive to the inclusion of dim sources. More specifically, we find that given the same level of cosmic star formation, the number of ionising photons required to reionise the Universe is overestimated by  $\sim 63\%$  when only objects with masses  $> 1.0 \times 10^9 h^{-1} M_{\odot}$  are used as source locations. This result stems from the fact that low-mass sources preferentially reside in less clumpy environments than their massive counterparts. Consequently, their exclusion has the net effect of concentrating more of the cosmic ionising radiation in regions which have higher recombination rates.

Our results from the full source list that includes objects down to  $M \sim 4.0 \times 10^7 h^{-1} M_{\odot}$  appear to show a similar evolution to reionisation for various values of the escape fraction. In all cases, the epoch of reionisation, which we define as occurring when the global volume-weighted ionisation fraction reaches 99%, happens by  $z \sim 7$ . This result is consistent with the absence of a Gunn-Peterson trough in observations of quasars below  $z \sim 6$ . To relate our results to these observations, we extract artificial Ly $\alpha$  absorption spectra from simulation outputs and then derive statistical probabilities for the resultant flux transmittance. Our comparisons are based on probability distribution functions involving transmission levels that have been averaged over the same redshift range as the observational measurements. Specifically, we focus on the redshift ranges  $5.95 < z < 6.16$  and  $5.74 < z < 5.95$ , corresponding to the regions over which the average transmittance

was measured by Becker et al. (2001) in the spectrum of their  $z = 6.28$  quasar. We find that given the amplitude and form of the underlying star formation predictions, an escape fraction near  $f_{esc} = 0.20$  is most consistent with the observational results. This leads to a reionisation epoch that is complete by  $z \simeq 7.8$  and requires roughly  $\sim 3$  ionising photons per hydrogen atom.

In an attempt to explore the implications arising from a scenario where sources with harder spectra such as AGNs are responsible for hydrogen reionisation, we have analysed a model in which the spectrum of sources is allowed to extend beyond 4 Ryd. As a result, sources are able to reionise He II simultaneously with H I. Our analysis shows that helium reionisation occurs near  $z \simeq 6.5$  when the spectrum is normalised to deliver the same number of H I ionising photons below 4 Ryd as predicted from soft sources with  $f_{esc} = 0.20$ . In a hypothetical case where these hard sources abruptly turn off before the onset of quasars below  $z = 5$ , we find that an early reionisation of the helium component is not necessarily in conflict with observational constraints of He II opacities obtained at  $z \simeq 3$ . This is due to the fact that by  $z \simeq 3$ , enough He III recombinations haven taken place to cause ionisation levels to converge to the values governed by quasar emissivities alone.

In this paper, we have focused on reionisation by stellar sources similar to those seen in local galaxies; i.e. population II type stars. Our results show that the star-formation history inferred by Springel & Hernquist (2003a) based on detailed hydrodynamic simulations can account for the properties of the IGM measured from quasars at  $z \gtrsim 6$ . To the extent that these comparisons are confirmed by future theoretical and observational studies, our results support the evolutionary history of “ordinary” star formation derived analytically by Hernquist & Springel (2003).

The recent measurements by the WMAP satellite (Kogut et al. 2003) indicate that a large fraction of the IGM may have been ionised early, by  $z \sim 14 - 20$ . Taken together with the observations of the SDSS quasars at  $z \sim 6$ , the implications of this result for the evolution of the IGM are unclear. Cen (2002) has proposed a scenario in which the Universe was reionised early by population III stars, but then much of the IGM recombined once these stars were no longer able to form, and the Universe was reionised a second time by the next generation of stars. Our results in this paper with a constant escape fraction would describe the second stage of reionisation in this model, provided that the IGM mostly recombined at intermediate redshifts.

Our models with a constant escape fraction predict a relatively late reionisation epoch and cannot account for the optical depth inferred by WMAP. In an effort to study how this difference could be reconciled in the context of population II type stars, we employed models with evolving escape fractions and found that if  $f_{esc}$  were to rise from  $f_{esc} = 0.20$

near  $z \simeq 6$  to  $f_{esc} \gtrsim 10$  near  $z \sim 18$ , the WMAP and SDSS constraints can both be satisfied. In this picture, an “escape fraction” larger than unity implies that the stellar production rate of ionising photons is much higher than that which would be produced according to our model assumptions. One mechanism that would boost the production rate of ionising photons would be if the IMF evolved so that it became more and more top-heavy with increasing redshift.

In the future, we will combine simulations of early structure formation with a detailed treatment of radiative transfer to investigate the combined effects of reionisation by both population III and population II stars. Preliminary work on related issues by Yoshida et al. (2003) indicates that dynamical heating by ongoing accretion limits the rate at which cold, dense clouds of molecular material can form in halos. In principle, this effect will severely reduce the rate of formation of massive stars through molecular cooling, perhaps rendering them unimportant as sources of ionising radiation. Dynamical simulations will be required to understand these processes in detail, and to reliably calibrate semi-analytical treatments, in a manner similar to the approach described here.

We thank Matias Zaldarriaga for discussions regarding the statistical significance of observational results in the context of our analysis. We also thank Brant Robertson for his services as a system administrator for the computer cluster used in this analysis. A.S. thanks Daniel Harvey for many constructive discussions related to this study. This work was supported in part by NSF grants ACI 96-19019, AST 98-02568, AST 99-00877, and AST 00-71019 and NASA ATP grant NAG5-12140. The simulations were performed at the Center for Parallel Astrophysical Computing at the Harvard-Smithsonian Center for Astrophysics.

## REFERENCES

- Abel T., Haehnelt M. G. 1999, ApJ, 520, L13
- Abel T., Wandelt B.D., 2002, MNRAS, 330, 53
- Anninos P., Zhang Y., Abel T., Norman M. L., 1997, New Astron., 2, 209
- Becker R.H., et al., 2001, AJ, 122, 2850
- Bennett, C.L. et al. 2003, ApJ, submitted [astro-ph/0302207]
- Bianchi S., Cristiani S., Kim T., 2001, A&A, 376, 1
- Cen, R. 2002, ApJ, submitted [astro-ph/0210473]
- Chiu W.A., Ostriker J.P., 2000, ApJ, 534, 507
- Ciardi B., Stoehr F., White, S.D.M., 2003a, preprint [astro-ph/0302451]
- Ciardi B., Stoehr F., White, S.D.M., 2003b, preprint [astro-ph/0301293]
- Cowie L. L., Songaila A., Kim T., Hu E. M, 1995, AJ, 109, 1522
- Djorgovski S.G., Castro S.M., Stern D., Mahaba A., 2001, ApJ, 560, 5
- Fan X., et al. 2000, AJ, 120, 1167
- Fan X., et al. 2001, AJ, 122, 2833
- Gnedin N.Y., 2000, ApJ, 535, 530
- Haardt F., Madau P., 1996, ApJ, 461, 20
- Haehnelt M.G., Madau P., Kudritzki R., Haardt F., 2001, ApJ, 549, L151
- Haiman Z., Abel T., and Madau, P., 2001, ApJ, 551, 599
- Haiman Z., Loeb A., 1998, ApJ, 503, 505
- Harris D. L., 1948, ApJ, 108, 112
- Heckman T.M., Sembach K.R., Meurer G.R., Leitherer C., Calzetti D, Martin C.L., 2001, ApJ, 558, 56
- Hernquist L., Springel V., 2003, MNRAS, in press [astro-ph/0209183]
- Hui L., Gnedin N. Y., 1997, MNRAS 292, 27
- Hurwitz M., Jenlinsky P., Dixon W. V., 1997, 498, L31
- Katz N., Quinn T., 1995, TIPS manual
- Kogut, A. et al. 2003, ApJ, submitted [astro-ph/0302213]
- Leitherer C., Ferguson H.C., Heckman T.M., Lowenthal J.D., 1995, ApJ 454, L19

- Madau P., Haardt F., Rees M.J., 1999, *ApJ*, 514, 648
- Miralda-Escudé J., Haehnelt M., Rees M.J., 2000, *ApJ*, 530, 1
- Osterbrock D. E., 1989, *Astrophysics of Gaseous Nebular and Active Galactic Nuclei* (Mill Valley: University Science)
- Razoumov A.O., Norman M.L., Abel T., Scott D., 2002, *ApJ*, 572, 695
- Schirber M., Bullock J.S., 2002, *ApJ*, submitted, astro-ph/0207200
- Sokasian A., Abel T., Hernquist, L. 2003, *MNRAS*, in press
- Sokasian A., Abel T., Hernquist, L. 2002, *MNRAS*, 332, 601
- Sokasian A., Abel T., Hernquist, L. 2001, *NewA*, 6, 359
- Spergel, D.N. et al. 2003, *ApJ*, submitted [astro-ph/0302209]
- Springel V., Hernquist L., 2002, *MNRAS*, 333, 649
- Springel V., Hernquist L., 2003a, *MNRAS*, 339, 312
- Springel V., Hernquist L., 2003b, *MNRAS*, 339, 289
- Steidel C. C., Pettini M., Adelberger K. L., 2001, *ApJ*, 546, 665
- Valageas P., Silk J., 1999, *A&A*, 347, 1
- Yoshida, N., Abel, T., Hernquist, L., Sugiyama, N., 2003, *ApJ*, submitted [astro-ph/0301645]
- Wood K., Loeb A., 2000, *ApJ*, 545, 86

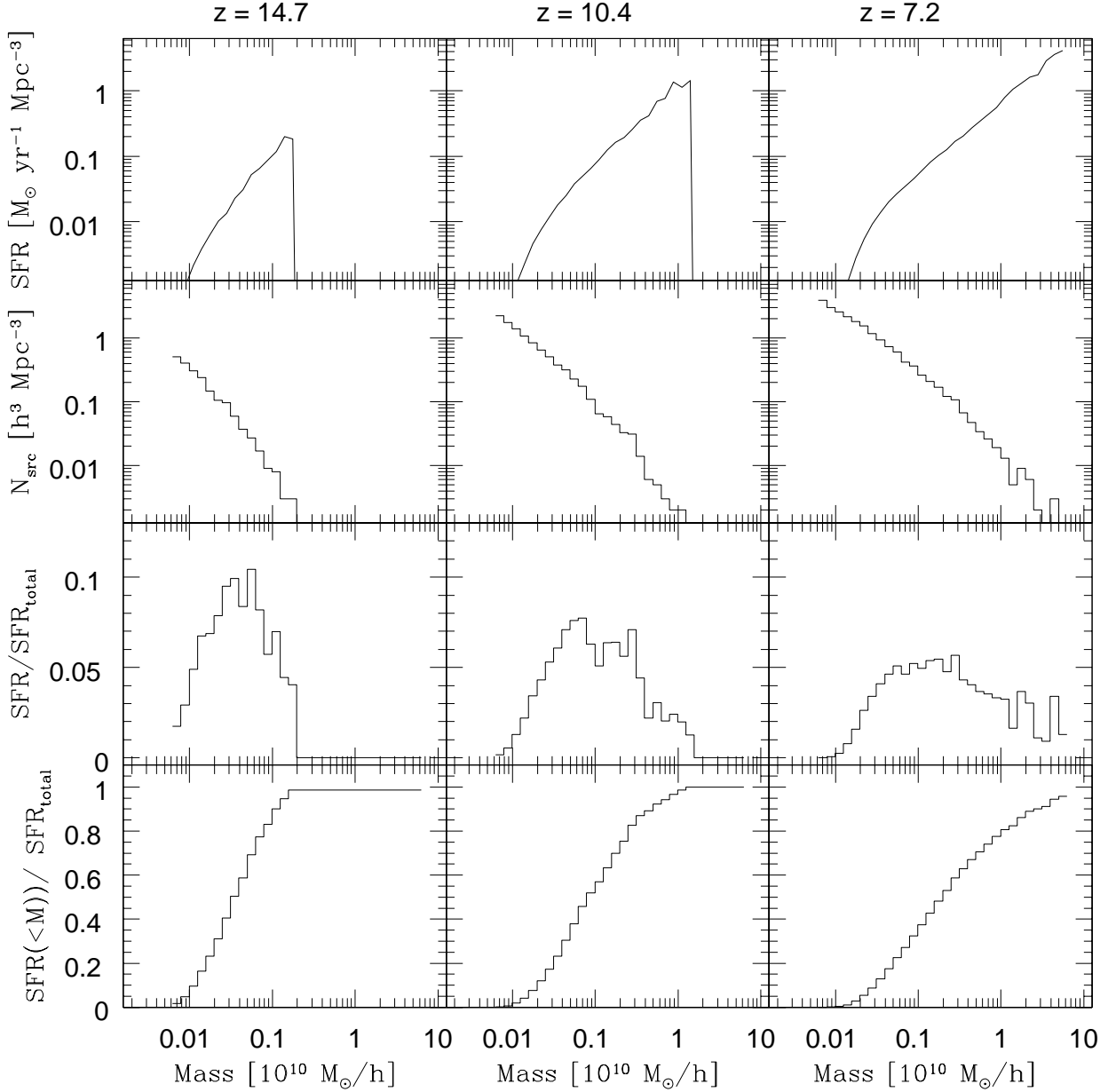


Fig. 1.— Statistics related to our raw source lists for redshifts  $z = 14.7$ ,  $10.4$  and  $7.2$ . The first row of panels show the star formation rate density as a function of total halo mass, demonstrating how star formation shifts to progressively larger mass scales with time. In the second row, we plot the comoving number density of halos in logarithmically spaced mass bins. The third row shows the fractional contribution to the total cosmic star formation rate at a given time for each mass bin. Note how at early times the contribution is heavily weighted towards the lower mass scales. Finally in the fourth row we plot the the cumulative fractional contribution to the total star formation from all halos below mass  $M$ .

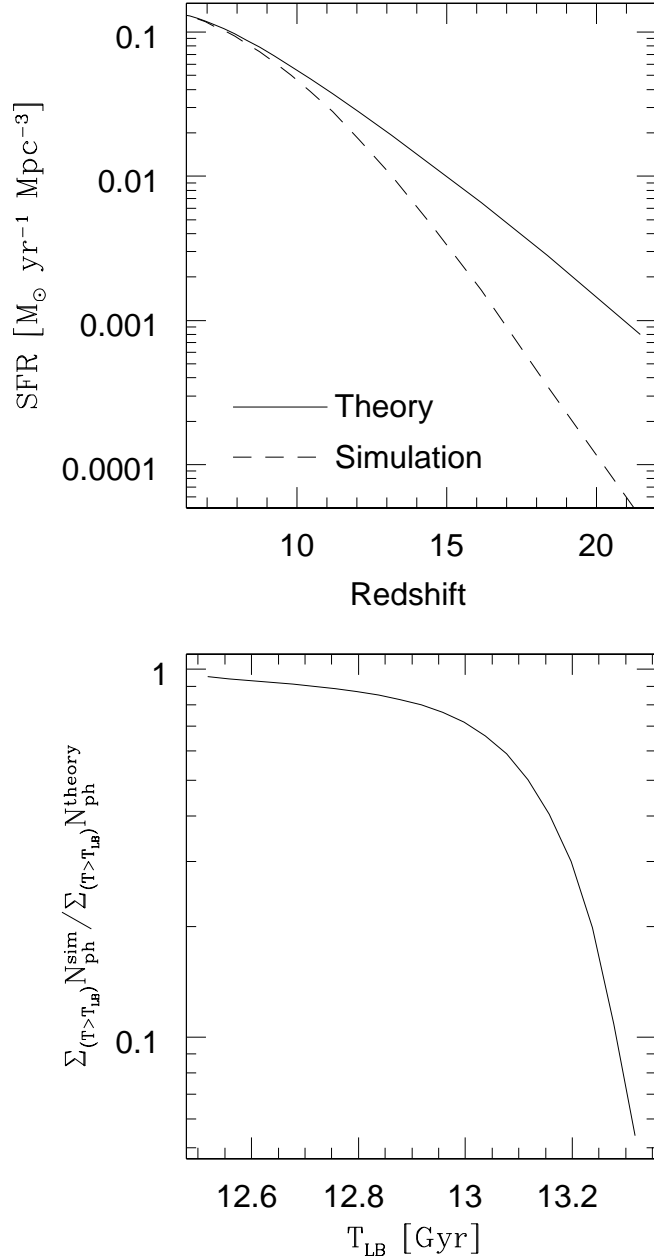


Fig. 2.— Comparisons between the computed simulation results for the cosmic star formation rate evolution and the theoretical prediction from the fit to the converged results from Springel & Hernquist (2003a) obtained by Hernquist & Springel (2003). In the top panel, we show the evolution in star formation rate as function of redshift for the two cases. In the bottom panel, we plot the ratio of the simulation result to the theoretical prediction in terms of the cumulative number of ionising photons released as a function of look-back time.

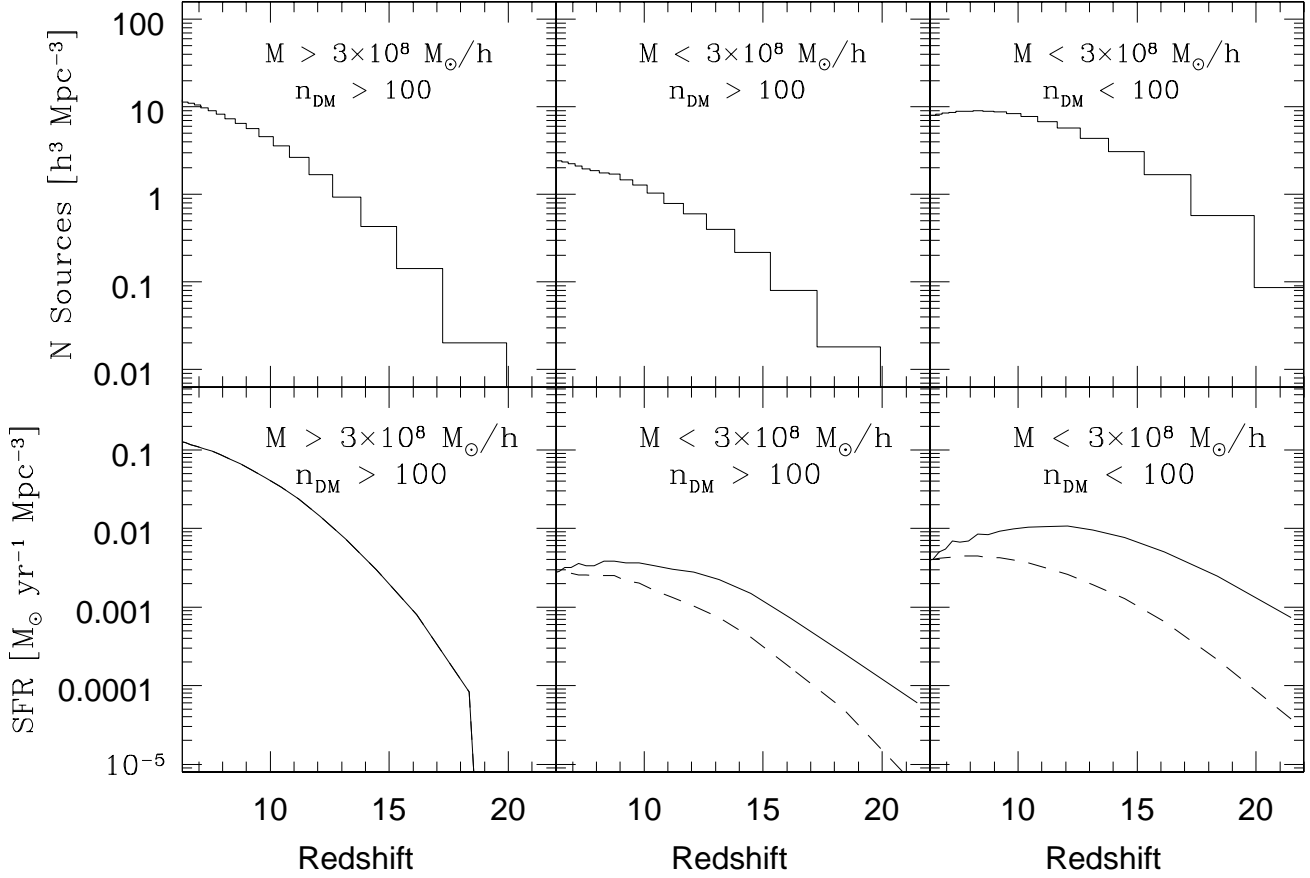


Fig. 3.— To study the resolution effects responsible for the deficit in the cosmic star formation rate relative to theoretical predictions, we have grouped the sources according to the number of dark particles and total mass in the associated halo. The top row of panels show source comoving number densities at each redshift bin. In the bottom row of panels we show the uncorrected (*dashed*) and corrected (*solid*) contributions to the cosmic star formation rate. The first column represents massive sources which are not affected by the limited resolution of the simulation. In the second column we have sources whose *reality* is not questioned ( $n_{\text{DM}} > 100$ ), but whose associated star formation rate may be underestimated due to the paucity of SPH particles associated with halos with  $M < 3.0 \times 10^8 h^{-1} M_{\odot}$ . And, finally, in the third column we have the case where both the halo’s existence is questionable and the associated star formation rate is underestimated. In the latter two cases, the star formation rate for each source was increased in proportion to the corresponding halo mass so that the total amount added equaled the deficit in the cosmic star formation rate (see text for discussion).



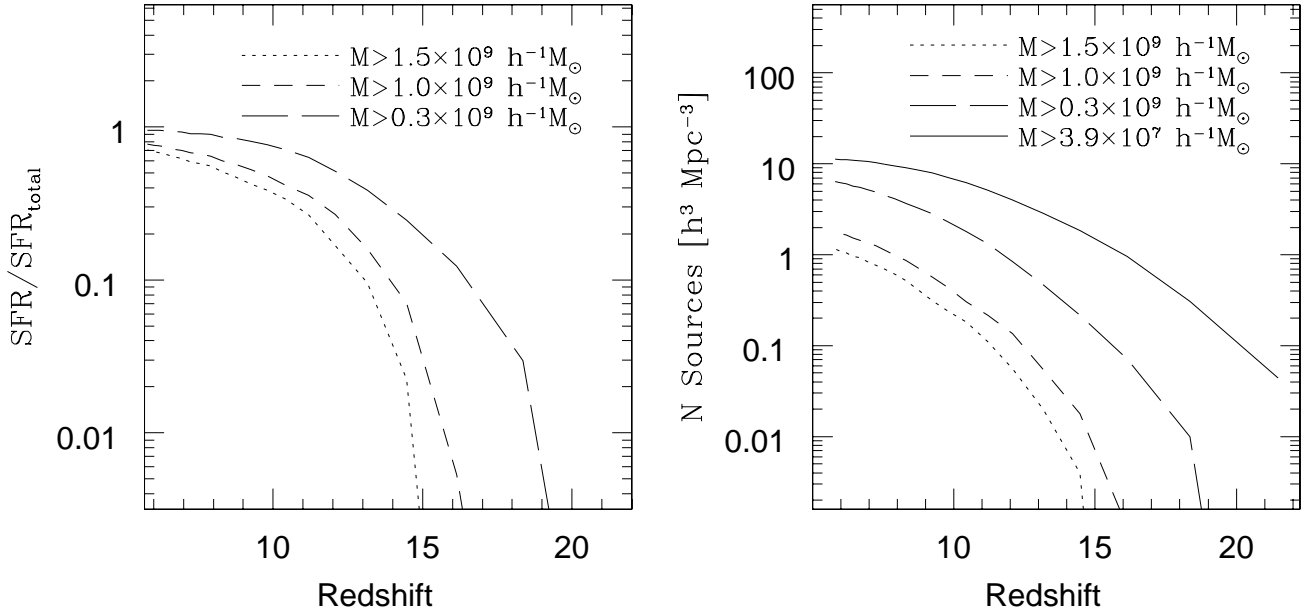


Fig. 4.— *Left panel:* Evolution of the fractional star formation rate when only objects above the labeled masses are included. The total SFR is taken from our own corrected source list which includes objects down to  $M \simeq 3.9 \times 10^7 h^{-1} M_{\odot}$ . *Right panel:* Comoving number densities of sources as a function of redshift for the same mass ranges. The total number density from our complete list of sources is also shown (*solid line*).

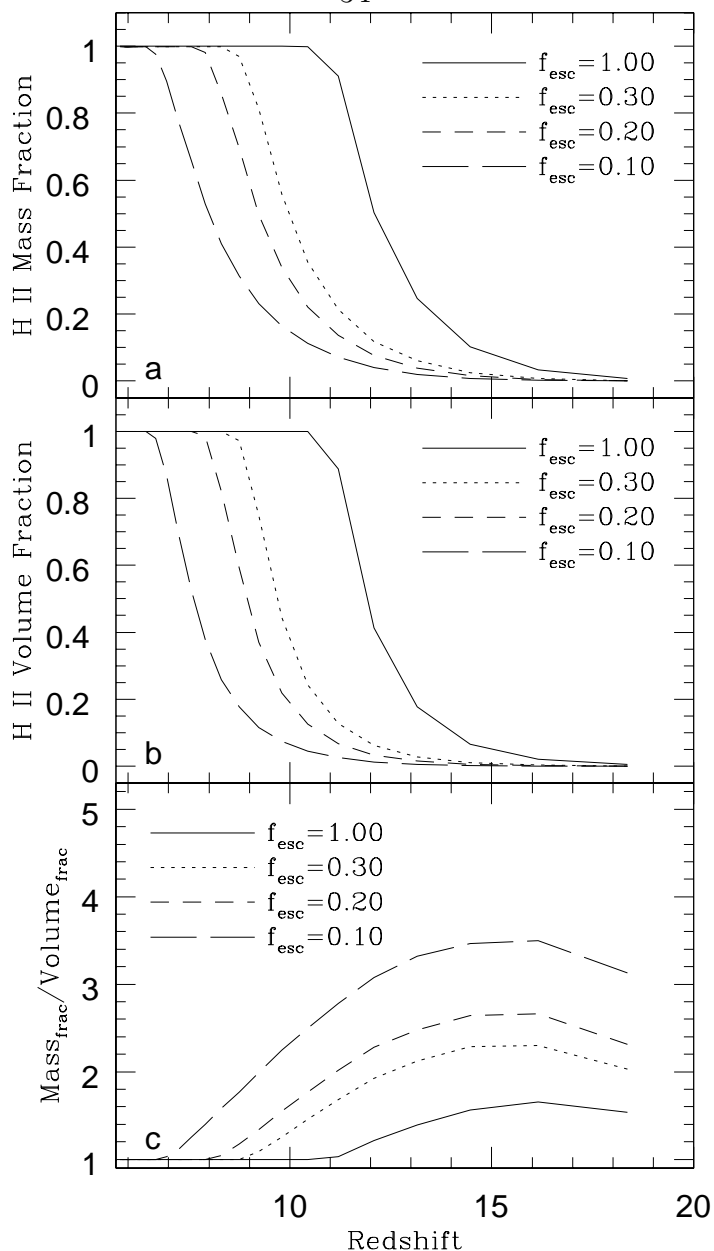


Fig. 5.— Evolution of the ionised mass-weighted fraction (a), ionised volume-weighted fraction (b), and the ionised mass to volume ratio (c) as a function of redshift for the labeled values of escape fractions. The epoch of reionisation is reached later with decreasing values of  $f_{esc}$  although the form of the evolution remains fairly similar in each case. Note also that the mass-weighted fraction is consistently greater than the volume-weighted fraction especially at early times when much of the ionising emissivity is preferentially concentrated in massive regions surrounding the sources.

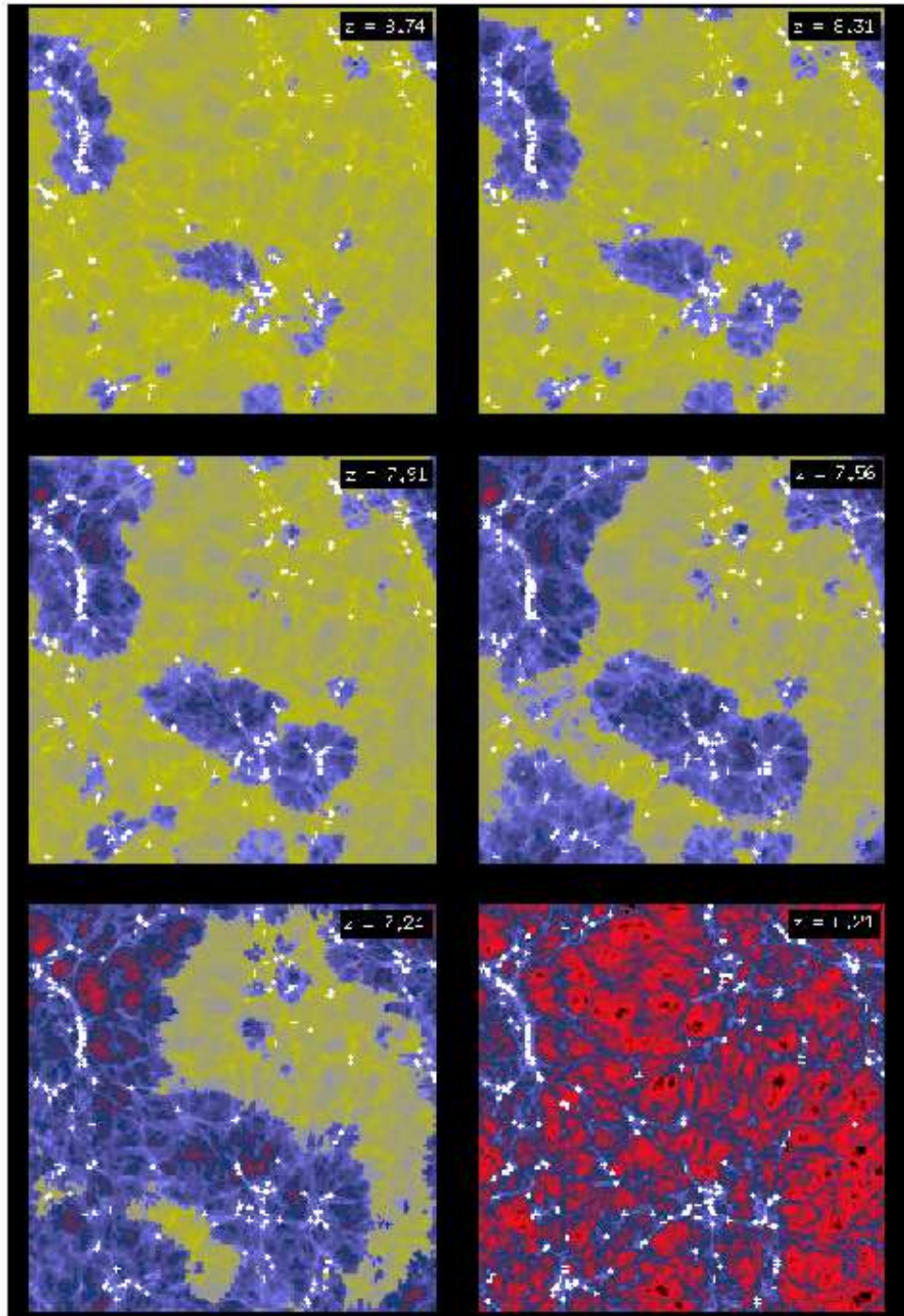


Fig. 6.— A series of projected slices through the simulation volume at (*top-left* to *bottom-right*)  $z=8.74$ ,  $8.31$ ,  $7.91$ ,  $7.56$ ,  $7.24$ , and  $6.21$ . In each panel, a  $0.25h^{-1}\text{Mpc}$  slice (1/40th of a box length) from the outputs of the  $f_{esc} = 0.10$  run is projected in both density and ionisation fraction. Source locations in each slice are denoted by white crosses making it easier to follow how the ionised regions (*blue*) percolate to turn a neutral IGM (*yellow*) into one that is highly ionised (*red*).

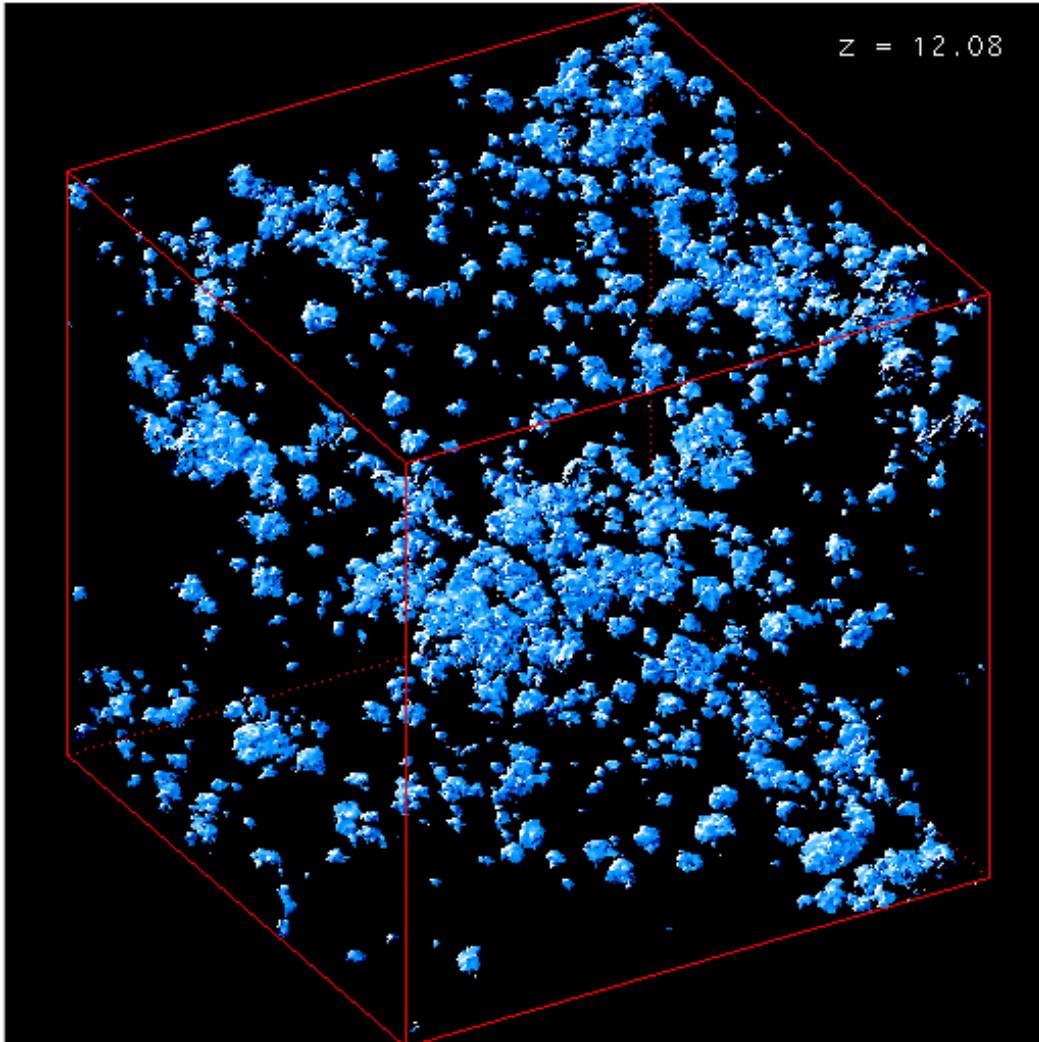


Fig. 7.— A 3D image showing iso-surfaces around ionised regions ( $\chi > 98\%$ ) at  $z = 12.08$  from the  $f_{esc} = 0.10$  model. The highly inhomogeneous morphology associated with how sources ionise their surroundings has a significant impact on the overall evolution of the reionisation process (see text for discussion).

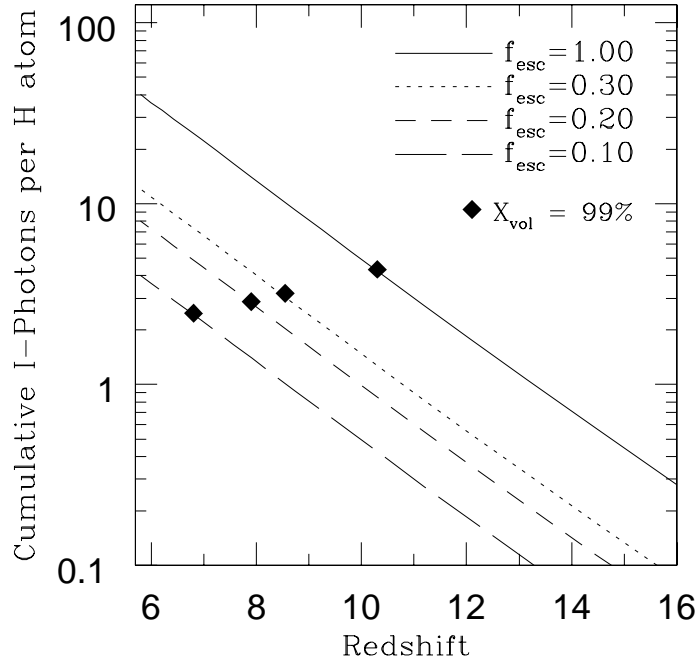


Fig. 8.— Cumulative number of escaping ionising photons per hydrogen atom as a function of redshift. The diamond symbol on each corresponding case of  $f_{esc}$  represents the point at which the volume-weighted ionisation fraction exceeds 99%, which is our criterion for the completion of the overlap epoch.

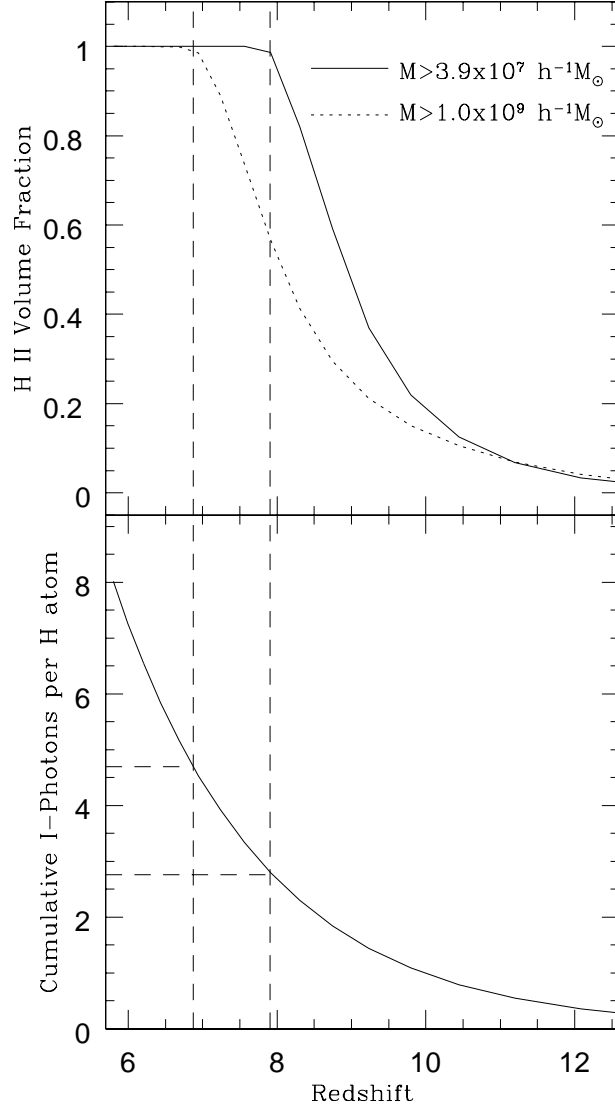


Fig. 9.— *Top panel:* Evolution of the volume-weighted ionisation fraction for the case where we have retained the full source list which includes sources down to our resolution limit of  $M \simeq 3.9 \times 10^7 h^{-1} M_{\odot}$  (*solid line*), and the case where we have systematically transferred ionising flux from sources below  $1.0 \times 10^9 h^{-1} M_{\odot}$  to the nearest neighbouring sources with masses above this limit (*dotted-line*). In both cases the escape fraction was set to  $f_{esc} = 0.20$ . *Bottom-panel:* Corresponding number of ionising photons released as a function of redshift. Note that the completion of overlap (*dashed-lines*) requires more ionising photons in the case where ionising flux is transferred away from low-mass sources (see text for discussion).

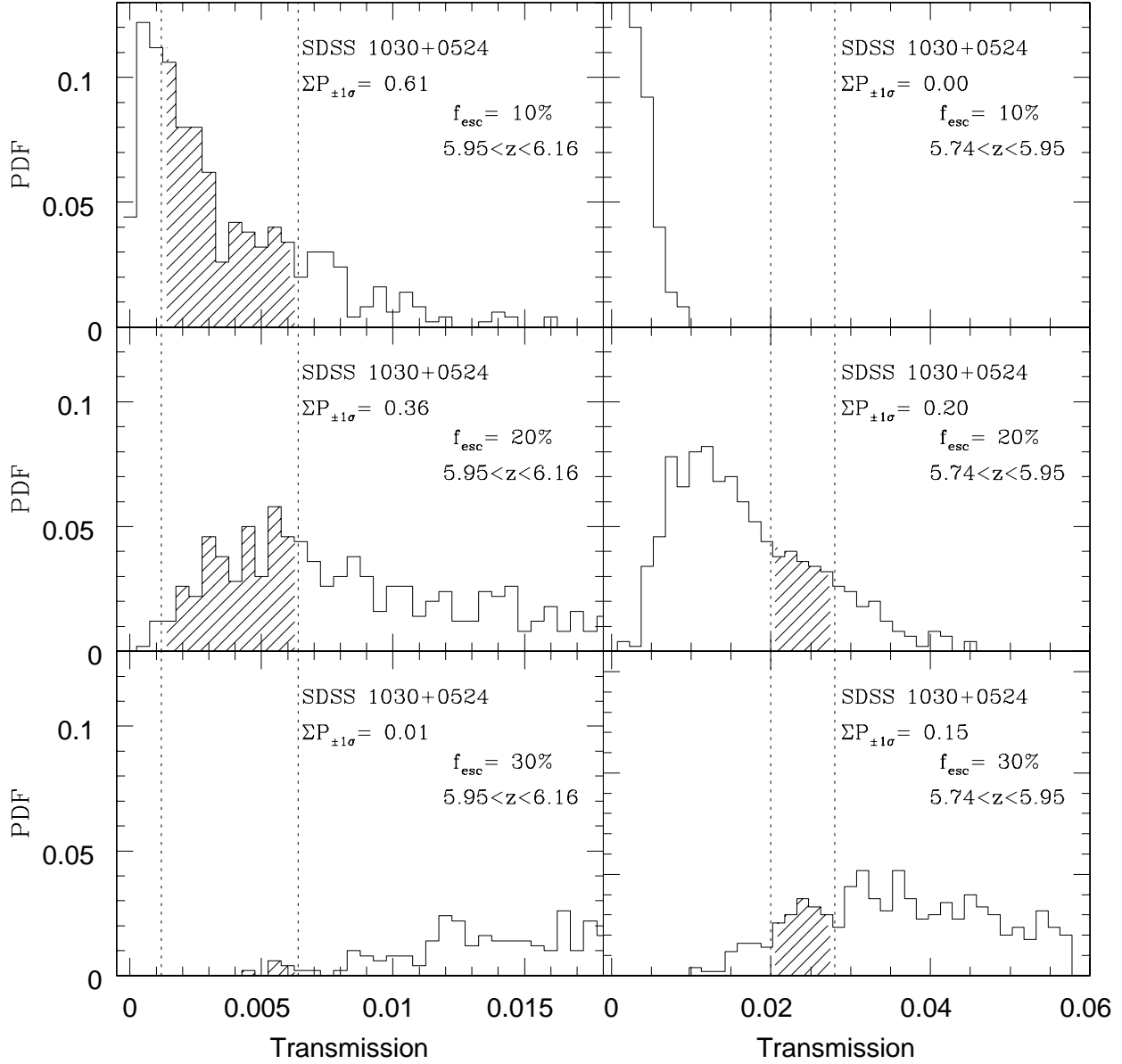


Fig. 10.— Probability distribution functions of the average transmission measured in the redshift ranges  $5.95 < z < 6.16$  (*left-column*) and  $5.74 < z < 5.95$  (*right-column*) computed using 500 LOS from our simulations for  $f_{\text{esc}} = 0.10, 0.20,$  and  $0.30$ . In each column, the range of transmissions shown is chosen on the basis of comparisons with the  $\pm 1\sigma$  measurements reported by Becker et al. (2001) for the  $z = 6.28$  quasar (*vertical-dotted lines*). The cumulative probability of measuring simulated transmissions consistent with the observations is represented by the shaded regions and numerically labeled in each panel.

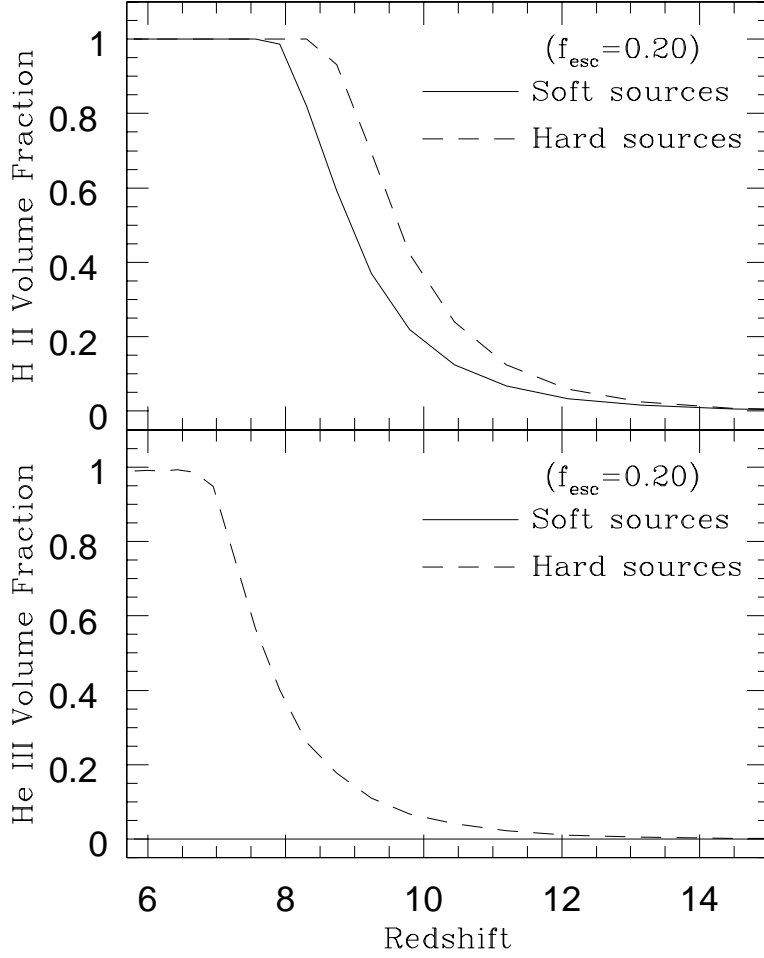


Fig. 11.— Evolution of the H II (*top*) and He III (*bottom*) volume-weighted ionisation fraction resulting from sources with a soft spectrum capable of ionising only hydrogen (stellar source model with  $f_{esc} = 0.20$ ; *solid-line*) and hard sources capable of ionising both hydrogen and helium (AGNs; *dashed-line*). He II ionising rates for the hard sources were computed assuming a spectrum of the form,  $f_\nu \propto \nu^{-1.8}$ , which is normalised to deliver the same number of H I ionising photons below 4 Ryd as predicted from soft sources with  $f_{esc} = 0.20$ . Hydrogen reionisation occurs earlier in the case where hard sources are invoked due to the additional H I ionising emissivity introduced from He II reionisation.



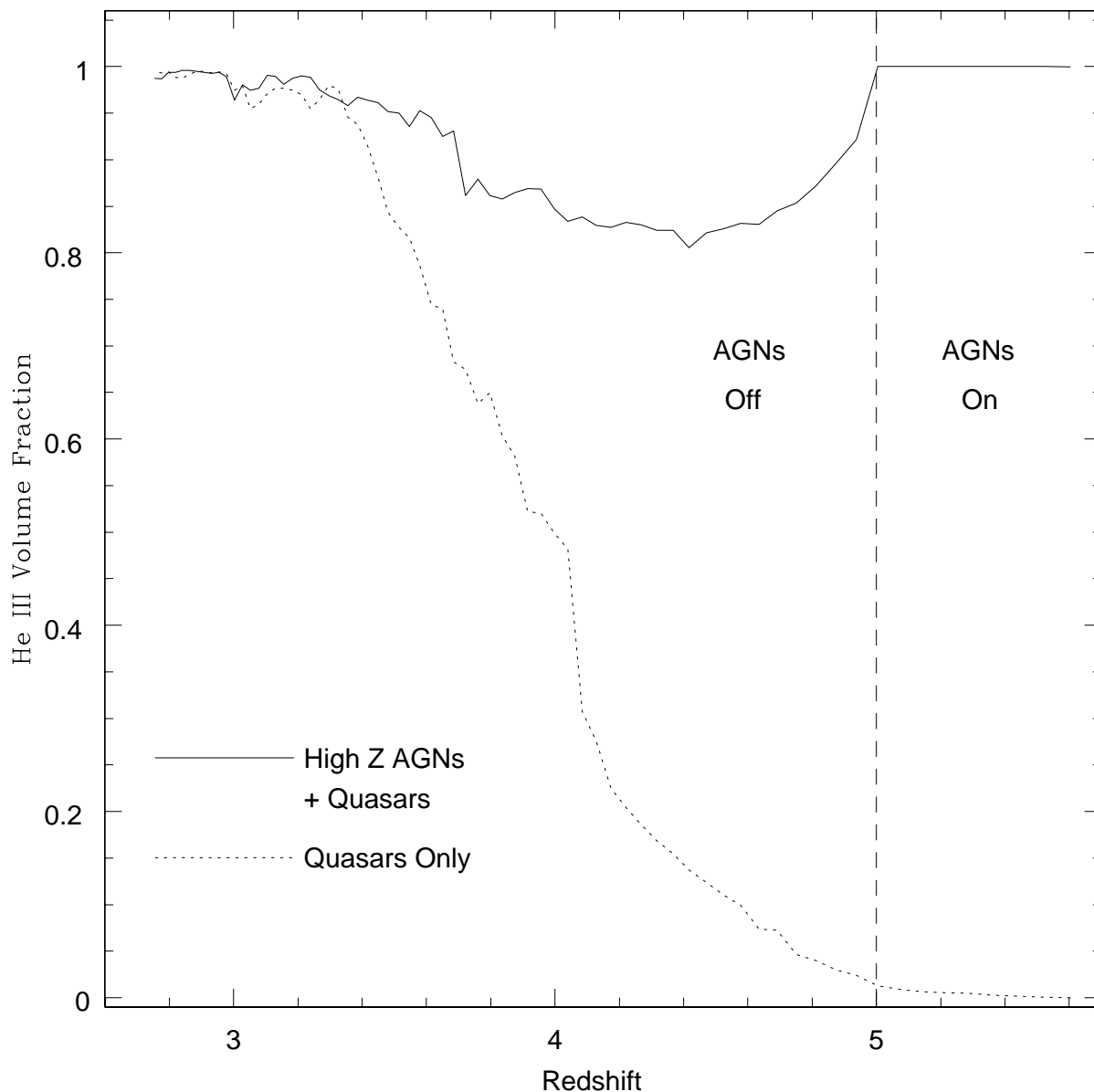


Fig. 12.— Evolution of the He III volume-weighted ionisation fraction due to quasars turning on at  $z < 5$ . The dotted line represents the results from the simulation conducted by Sokasian et al. (2002) involving a realistic quasar model (model 5). The solid line shows the resultant evolution in the same simulation now involving the scenario where the IGM was first highly ionised due to the presence of hard sources (such as AGNs) which abruptly turn off at  $z = 5$ . Note the ionisation fraction in the latter case eventually converges to the same levels as in the case involving quasars only, rendering it indistinguishable in light of current observational results for He II opacities near  $z \simeq 3.2$  (see Sokasian et al. 2002).

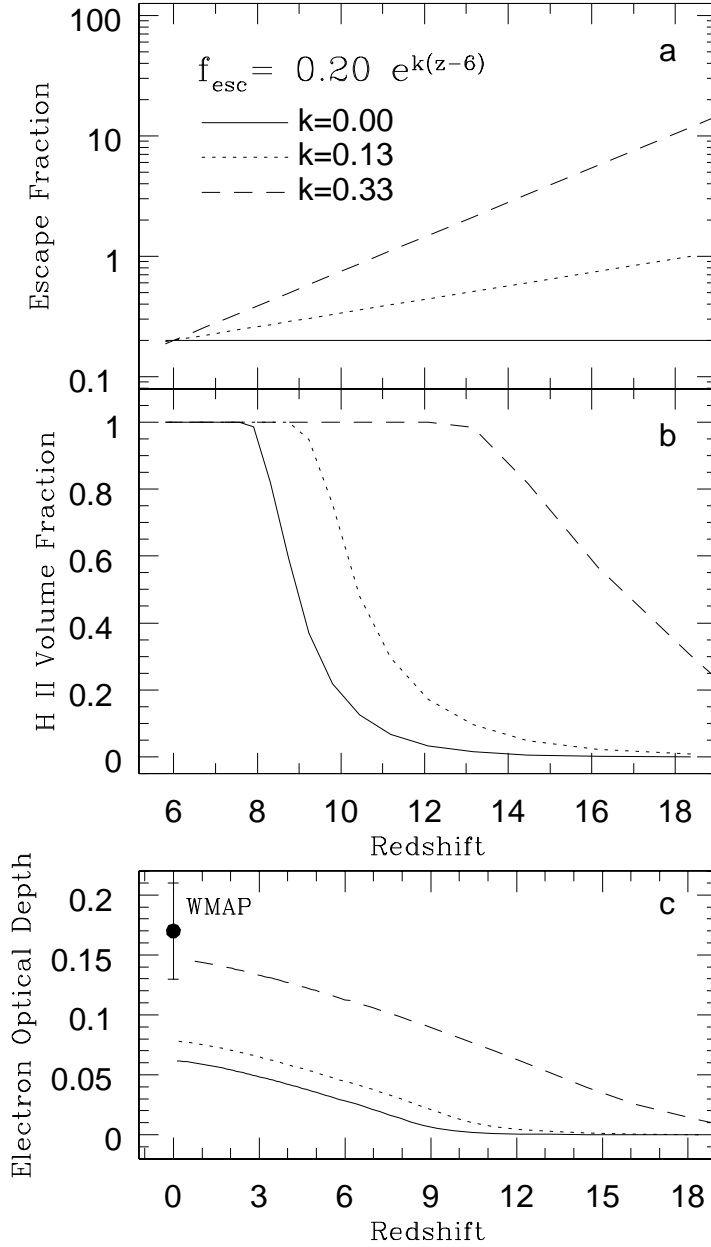


Fig. 13.— Redshift evolution of the escape fraction (a), H II volume-weighted ionisation fraction (b), and electron optical depth (c) for the case with a constant escape fraction of  $f_{\text{esc}} = 0.20$  (*solid-line*), and two cases where we have adopted an evolving escape fraction of the form  $f_{\text{esc}}(z) = 0.20e^{k(z-6)}$ . The case with  $k = 0.13$  (*dotted-line*) represents the scenario where there is an evolution of the escape fraction from 0.20 at  $z = 6$  (necessary to provide a consistent match with the Becker et al. 2001 observations) to unity at  $z = 18$  around when the first star-forming sources turn on. The case with  $k = 0.33$  results in an escape fraction which is larger than unity beyond  $z \gtrsim 11$  and is meant to serve as an illustrative example of the additional ionising flux necessary at high redshifts in order to match the electron optical depth measurement implied by the Kogut et al. (2003) “model independent” analysis (WMAP data point in panel c).